Geological controls on fault relay zone scaling

Jonathan J. Long*[1] and Jonathan Imber[1]

[1]Department of Earth Sciences, Durham University, Durham, UK

*Corresponding author: jonathan.long@durham.ac.uk

Abstract:

The overlap and separation distances of relay zones follow a power-law scaling relationship over nearly 8 orders of magnitude. Approximately one order of magnitude scatter in both separation and overlap exists at all scales. The strong power-law relationship (R^2=0.98) suggests that the primary control on relay aspect ratio (overlap/separation) is a scale-invariant process, such as the stress interaction between the overlapping fault tips as suggested by previous authors. Host rock lithology is not a first order control. Much of the observed scatter can be attributed to the spread of measurements recorded from individual relay zones, which relates to the evolving three-dimensional geometry of the relay zone as displacements on the bounding faults increase. Relay ramps exposed at two localities where the faults cut layered sedimentary sequences display mean aspect ratios of 8.20 and 8.64 respectively, more than twice the global mean (4.2). Such high aspect ratios can be attributed to the relay-bounding faults having initially been confined within competent layers, facilitating the development of large overlap lengths. The presence of pre-existing structures (veins) at fault tips may also enhance fault propagation, giving rise to increased overlap lengths.

Keywords:

Scaling; relay zone; fault interaction; aspect ratio; and stress field.

1   Introduction

Fault arrays comprise multiple fault segments at all scales (Peacock and Sanderson, 1991; Childs et al., 1995; Childs et al., 1996a; Willemse, 1997; Crider and Pollard, 1998; Peacock, 2002). As the fault-array grows these segments overlap to form relay zones (Fig. 1a), which are dynamic structures that evolve with increased displacement (Peacock and Sanderson, 1994; Childs et al., 1995; Walsh et al., 1999). The linkage of fault segments at relay zones is a fundamental process by which faults grow (Cartwright et al., 1996; Walsh et al., 2003). In map view, different stages in the evolution of relay ramps have been recognised. Relay ramps initiate as open structures with a continuous relay ramp linking the footwall and hanging wall (Fig. 1a) (Peacock and Sanderson, 1994). As displacement on the bounding faults increases, the ramp continues to rotate (i.e. to accommodate shear strains) and linking faults begin to grow. Finally, a through going fault is formed producing a breached relay ramp (Fig. 1b and c). It is inferred that different stages of relay ramp evolution can coexist within a single relay zone (Peacock and Sanderson, 1994; Long and Imber, in review).

The geometry of a relay ramp is most commonly described in terms of its aspect ratio, which is the ratio between the fault overlap and separation, as measured in map view on a particular stratigraphic horizon (Fig. 1) (Aydin and Schultz, 1990; Huggins et al., 1995; Acocella et al., 2000; Soliva and Benedicto, 2004). Published datasets of relay ramp aspect ratios show a power-law scaling relationship between overlap and separation, with mean relay aspect ratios ranging from 4 to 4.9 (Aydin and Schultz, 1990; Huggins et al., 1995; Acocella et al., 2000; Soliva and Benedicto, 2004). In these global relay datasets, there is approximately one order of magnitude scatter around the trend line at all scales. A proportion of this scatter may arise from the different techniques used to define and measure fault overlaps and separations in disparate outcrop and seismic reflection datasets, each with different resolutions and at different scales of observation. We describe an approach to reduce the main sources of sampling-related error before presenting a refined global dataset. This refined dataset comprises a consistent set of overlap and separation measurements from relays observed in three-dimensional (3D) seismic surveys, outcrops and selected published sources. Any remaining scatter within the refined dataset should primarily reflect geological processes, rather than measurement errors or inconsistencies

57   between disparate datasets. We use this refined dataset to propose a simple mechanical

58   model, which explains the overall power-law relationship between fault overlap and

59   separation distances in relay zones. We then investigate the geological causes of scatter

60   within the refined global dataset. An important difference between this and previous

61   studies (e.g. Aydin and Schultz, 1990; Acocella et al., 2000; Soliva and Benedicto, 2004) is

62   that we focus on the role played by the 3D geometric variability of individual relay zones

63   (e.g. Kristensen et al., 2008). We conclude that processes attributed to relay zone growth

64   and linkage, and the influence of mechanical stratigraphy and pre-existing heterogeneity are

65   the main causes of scatter within the overall power-law scaling relationship.

2   Criteria to identify and measure fault overlap and separation

68   In the context of this paper, uncertainty occurs when multiple interpretations can be drawn

69   from the same data and a unique interpretation cannot be ascertained. Errors in

70   measurement are those arising due to sampling related inaccuracies or inconsistencies. The

71   main sources of error or inconsistency are related to accurately locating the positions of the

72   relay-bounding faults and their lateral tips in disparate datasets (outcrops and 3D seismic

73   surveys). In the following section, we explain how methods developed by Long and Imber

74   (2010; in review), which permits measurements of both the continuous and discontinuous

75   components of fault-related deformation (Walsh et al., 1996; Walsh et al., 2003), can be

76   used to derive a consistent set of overlap and separation measurements from relay zones

77   observed in outcrop and 3D seismic data.

2.1   Fault overlap

79   Overlap is defined as the distance between the tips of the relay-bounding faults, measured

80   parallel to the strike of the faults on a given stratigraphic horizon (Fig. 1a). In linked

81   (breached) relay ramps, overlap is measured from the branch point to the fault tip (Fig. 1b),

82   or branch point to branch point (Fig. 1c). Measuring overlap length thus depends on

83   accurately locating fault tips and branch points. Branch points are the intersections between

84   two faults. Displacements at branch points are non-zero. Therefore, in datasets which have

85 limited vertical and horizontal resolution, such as 3D seismic surveys, the errors in locating

86 fault tips are likely to be greater than those for locating branch points (Long, 2011; Long and

87 Imber, in review). In suitable outcrops, fault tips can be observed directly, whereas in

88 seismic data there is an inherent resolution limit below which discrete fault geometries

89 cannot be imaged (Steen et al., 1998; Townsend et al., 1998). Therefore, outcrop

90 observations are used to develop simple criteria for identifying the location of fault tips. The

91 same criteria are then used to identify the tips of fault zones mapped using 3D seismic

92 reflection datasets.

93 2.1.1   Criteria to locate fault tips at different scales of observation

94 2.1.1.1   Outcrop scale examples - Kilve

95 Two examples of fault tips associated with a centimetre-scale relay zone from Kilve, UK, are

96 shown in Fig. 2. For details of the tectonic and sedimentary history of Kilve, see (Peacock

97 and Sanderson, 1991, 1992, 1994) . The throws on faults F1 and F2 decrease laterally and

98 terminate within pre-existing veins (Crider and Peacock, 2004). The magnitude of

99 continuous deformation (reverse drag or fault propagation folding) around these faults is

100 negligible, and the tips can be located with a high degree of accuracy from (throw)

101 displacement vs. distance plots (Fig. 2b).

102 Fig. 3 shows the tip of a metre-scale fault zone from Kilve (maximum displacement > 2.5 m).

103 In map view (Fig. 3b), the fault passes laterally into a monocline. Bed rotations within the

104 monocline are facilitated by shearing of the surrounding shale layers and by development of

105 wedge-shaped veins within the limestone bed (Fig. 3a). The vertical deflection of the

106 limestone bed across the monocline can be measured by hand in the field or, more

107 effectively, by obtaining measurements from terrestrial laser scans of the deformed bedding

108 surface (Long, 2011; Chapter 2). The total vertical displacement (throw) on the fault and

109 adjacent monocline decreases monotonically towards the west (Fig. 3d), indicating that the

110 fault and monocline are part of a single, coherent fault zone (sensu Walsh and Watterson,

111 1991; Walsh et al., 1996). In this case, the "true" tip of the fault zone is situated at the

112 lateral termination of the monocline, approximately 20m west of the point at which the

113 fault scarp disappears (Fig. 3d). A similar situation pertains to fault zones mapped in 3D

114 seismic reflection datasets, as described below.

2.1.1.2 Seismic scale example - Inner Moray Firth

Long and Imber (2010; their Figs. 8 and 9) have shown that seismically-resolvable normal faults that cut sub-horizontal sedimentary sequences pass laterally into bands of continuous deformation (monoclinal folding and/or sub-seismic scale faulting; Steen et al., 1998; White and Crider, 2006). Added together, the continuous and discontinuous deformation define a coherent fault array (Walsh et al., 1996; Long and Imber, 2010). The location of the "true" fault tip is assumed to be the point at which the total vertical displacement (fault throw + continuous deformation) reaches zero. Fig. 4 shows the aspect ratios measured on different stratigraphic horizons within a single relay zone from the Inner Moray Firth, Scotland (Fig. 4). The grey line shows the aspect ratios calculated using fault overlap lengths based on locating the fault tips using plots of fault throw vs. distance (i.e. the standard method used to define the location of fault tips). Using plots of *total* vertical displacement (i.e. vertical displacement due to fault-related folding + fault throw) vs. distance in order to locate the "true" tips of the relay-bounding faults increases the aspect ratio by approximately 1.1 at all depths within the relay zone (Fig. 4: black line). We have therefore used plots of total vertical displacement vs. distance to obtain the "true" fault tip locations, hence a consistent set of relay overlap lengths, in all the data derived from outcrop and seismic examples presented in this paper (Fig. 5).

2.2 Fault separation

Fault separation is defined as the perpendicular distance between two overlapping fault segments, measured at the centre of the relay zone (Fig. 1). There are two main sources of error in this measurement: (1) correctly identifying the centre of the relay zone; and (2) correctly locating the primary relay-bounding fault surfaces within a potentially wide zone of fault-related deformation. Locating the centre of a relay zone depends on knowing the overlap length. Therefore, errors in establishing the fault overlap length will alter the location at which separation is recorded. Separation has therefore been measured after the "true" tips of the relay-bounding fault zones have been established.

2.2.1 Criteria to locate the primary relay-bounding faults within a zone of fault-related deformation

Long and Imber (2010; in review) have shown that fault planes mapped in 3D seismic data are surrounded by volumes of continuous deformation that vary in width in both the strike and dip directions of the fault. These volumes of continuous deformation can be asymmetrically distributed between the hanging wall and footwall and may comprise more than 50% of the total vertical displacement across a fault zone. In all cases, however, the continuous deformation is an integral component of the coherent fault array (Walsh et al., 1996; Long and Imber, 2010; Long, 2011; Long and Imber, in review) .

In this study, the principal relay-bounding faults are taken as laterally continuous structures on which the majority of the offset is accommodated. In settings where the fault traces can be mapped directly (e.g. in outcrop or some 3D seismic datasets), fault separation is measured between the centres of the mapped fault polygons (Fig. 1d). In relay zones where the bounding faults are identified solely by zones of continuous deformation (e.g. in many 3D seismic datasets; see Long and Imber, 2010; their fig. 9 horizons H1-H3) the separation is measured between the centres of laterally continuous monoclines with the largest measured deflections i.e., between the inferred fault traces (Fig. 1e). Nevertheless, monoclines can range in width from 50 to 300 m and the precise location of the main fault trace cannot always be inferred. Fault separation could therefore be under or over estimated by an amount up to half of the width of the monocline (Fig. 1f). At present, there is no way to ascertain the unique distribution of faults below the resolution of seismic data and therefore these uncertainties cannot be mitigated.

3 First order trends in the global dataset of relay zone aspect ratios

Fig. 5a shows the global dataset of relay zone overlaps and separations. The data are all derived from faults in extensional terrains and include measurements from selected literature sources (diamonds), in addition to new measurements obtained during the present study (circles). The new measurements have been obtained from relay zones

170   mapped using 3D seismic data (Inner Moray Firth, offshore Scotland; Laminaria High, NW

171   Shelf of Australia; and Miskar, Gulf of Gabès, offshore Tunisia; n = 161), terrestrial laser

172   scans of centimetre- to metre-scale relays exposed onshore (Kilve and Lilstock, Bristol

173   Channel, UK; and Lamberton, Berwickshire, UK; n = 52) and high-resolution digital elevation

174   models of larger metre- to decametre-scale relays exposed onshore (Bishop Tuff, California;

175   and Arches National Park, Utah; n = 12). These measurements have been made in

176   accordance with the criteria outline in section 2 (i.e. continuous deformation has been

177   included in order to define fault overlap and separation). The raw data are provided in the

178   Supplementary Material and the background geology of each area is summarised by Long

179   (2011). The data from the literature sources have been derived from (Barnett et al., 1987;

180   Larsen, 1988; Morley et al., 1990; Cartwright, 1991; Roberts and Jackson, 1991; Stewart and

181   Hancock, 1991; Gawthorpe and Hurst, 1993; Anders and Schlische, 1994; Peacock and

182   Sanderson, 1994; Trudgill and Cartwright, 1994; Childs et al., 1995; Huggins et al., 1995;

183   Walsh et al., 1999; Acocella et al., 2000; Gupta and Scholz, 2000; McLeod et al., 2000;

184   Peacock et al., 2000; Cowie and Roberts, 2001; Morley, 2002; Peacock et al., 2002; Soliva

185   and Benedicto, 2004; n = 291). The raw data are provided in the Supplementary Material.

186   The literature-derived data in Fig. 5a have not been corrected for measurement errors or

187   inconsistencies (section 2). Nevertheless, there is a clear power-law relationship between

188   relay overlap and separation that spans nearly 8 orders of magnitude in separation distance.

189   As noted by previous authors, there exists approximately 1 order of magnitude scatter in

190   both overlap and separation at all scales of observation (Fig. 5a).

191   Fig. 5b demonstrates the effect of including continuous deformation in obtaining

192   measurements of fault overlap and separation, using examples from the Inner Moray Firth

193   and Laminaria High. Accurate location of the "true" fault tips using total displacement vs.

194   distance plots (section 2) has caused a shift towards greater overlap lengths, by

195   approximately a factor of 1.5 for relays mapped using 3D seismic data (Fig. 5c). Fault

196   separation measurements for some relay zones also changed when continuous deformation

197   was included, because an increase in overlap length changed the point at which relay

198   separation was measured (Fig. 5c). A correction factor of 1.5 has therefore been applied to

199   all literature-derived fault overlap measurements, where the relay zones have been mapped

200   from 3D seismic data. This correction incorporates the zone of coherent, continuous

201   deformation that is likely to exist beyond the mapped fault tips. Literature-derived fault

202   overlap measurements obtained from relays measured in outcrop have not been corrected:

203   unless specifically stated in the source paper, it is assumed that monoclines and/or minor

204   structures at fault tips would have been included in the measurements of fault overlap

205   length.

206   The refined global dataset also displays a clear power-law relationship between overlap and

207   separation that again spans nearly 8 orders of magnitude (Fig. 5d). The best-fit power-law

208   trend line is $y=3.634x^{0.97}$ $R^2=0.98$ and the mean aspect ratio of 4.2 and a standard deviation

209   of 3.0. The extent of the observed scatter in the refined global dataset is approximately the

210   same as the unrefined dataset: that is, an order of magnitude in both overlap and

211   separation across the entire measured scale range (Fig. 5c). Nevertheless, this correction

212   gives us confidence that: (1) the observed correlation between overlap and separation is

213   genuine; and (2) that the remaining scatter is primarily caused by geological processes, not

214   measurement errors or inconsistencies.

215   More detailed analyses of the overall controls on the power-law scaling and scatter are

216   provided below, but three key points are immediately evident from inspection of the

217   refined global dataset. First, separating individual data points by the dominant host-rock

218   lithology shows that no systematic relationship exists between lithology and relay aspect

219   ratio (Fig. 5d). Thus, host rock lithology is not a first-order control on relay aspect ratio.

220   Second, relays from particular locations, whether those sampled for this study or those

221   acquired from literature sources, often display a spread of relay ramp measurements that

222   fill the observed scatter range (Fig. 5d). Third, relay ramps at two of the field localities in this

223   study (Kilve and Lamberton) both systematically plot above the global trend line and have

224   higher than mean aspect rations, of 8.20 (standard deviation = 4.9) and 8.64 (standard

225   deviation = 4.5) respectively, when compared to the global mean aspect ratio (4.2). Relay

226   aspect ratios from these outcrops are also greater than other outcrop-scale relays from

227   literature sources of similar scales and quality of outcrop exposure (Fig. 5d) (Peacock and

228   Sanderson, 1994; Gupta and Scholz, 1998; Acocella et al., 2000; Gupta and Scholz, 2000).

229   These observations suggest there may be location-specific controls on relay ramp geometry.

4   Geometries of individual relay zones

The global relay dataset can be filtered to show the changes in relay ramp aspect ratio with depth throughout individual relay zones mapped using 3D seismic reflection data (Fig. 6). The overlaps and separations of relay-bounding faults surrounding individual relay zones span up to the entire range of scatter observed in the global dataset (Fig. 6a). Three main trends can be identified from this data: type one, relay zones have a wide spread in overlap length but a narrow range in separation values (dashed black lines defining sub-vertical ellipses in Fig. 6a); type two, relay zones have similar spreads in both overlap and separation lengths (solid grey lines defining circles in Fig. 6a); and type three, relay zones have a wide spread in separation length but a narrow range in overlap length (solid black lines defining sub-horizontal ellipses in Fig. 6a).

The same data have been re-plotted as aspect ratio against normalised depth in Fig. 6b in order to show how the observed trends in overlap and separation measurements relate spatially. In general, type one relay zones (Fig. 6: dashed black lines) can be described as having low aspect ratios at the upper and lower parts of the relay zone (i.e. toward the upper and lower tip lines of the relay-bounding faults) and relatively high aspect ratios in the centre. An example of this type of relay zone is shown in Fig. 4, which is comprised of two overlapping semi-planar fault segments. The upper and lower tip lines retreat upwards and downwards respectively, and appear elliptical in strike projection (Fig. 7a). Type two relay zones (Fig. 6: solid grey lines) can be approximated to relay zones with relatively uniform aspect ratios with depth. The tip lines of the overlapping relay-bounding faults are sub-vertical and display only slight curvature (retreat) at the top of the relay zone compared to type one relays (Fig. 7b). Finally, type three relay zones can be described as having relatively low aspect ratios in the upper sections of the relay zone and comparatively large aspect ratios in the lower sections of the relay zone. Relay Laminaria east R9, for example, displays an increase in aspect ratio with depth throughout the relay zone (Fig. 6b). The relay-bounding faults, for Laminaria east R9, are also linked along branch lines (Fig. 7c).

Not all relay zones conform to these idealised geometries. For example, the Laminaria east R7 relay zone has relatively large aspect ratios, of 6.8 to 8.4, in the upper and lower sections of the relay zone but has aspect ratios, of 4.4 to 4.7, in the centre of the relay zone (Fig. 6b).

260 Such variations can be ascribed to partially-breached relay zones in which the relay-
261 bounding faults are linked along branch lines at certain stratigraphic levels, but retain free
262 tips above and below (Fig. 7d) (Imber et al., 2004). The stratigraphic levels at which linkage
263 occurs could be related to the mechanical properties of the host stratigraphic sequence,
264 which can influence how strains are accommodated (Ferrill and Morris, 2008). However, we
265 do not have the data required to test this hypothesis in the Laminaria east R7 example (e.g.
266 detailed well log calibration).

267 To summarise, variations in the geometries of the relay-bounding faults (tip line shape, fault
268 surface geometry and location and continuity of branch lines) within a single relay zone can
269 account for much of the observed scatter within the refined global dataset of relay aspect
270 ratios. In the following section, we discuss the possible controls on the overall power-law
271 relationship between fault separation and overlap in relay zones. We then propose a simple
272 kinematic model to explain the variations in relay zone geometry that account for much of
273 the observed scatter. Finally, we consider the role of mechanical stratigraphy and
274 lithological heterogeneity to explain the unusually high aspect ratios recorded in relay
275 ramps exposed at Kilve and Lamberton.

276 # 5   Discussion

277 ## 5.1   Global scaling of fault overlap and separation in relay zones

278 The power-law relationship between fault overlap and separation in relay zones suggests
279 that the primary control on relay zone geometry scales with the size of the relay-bounding
280 faults (Fig. 5). We propose that Gupta and Scholz's (2000) elastic-plastic model of fault
281 interaction can explain this first order scaling relationship. In the model, the relay-bounding
282 faults interact through their overlapping stress fields, and little or no interaction is expected
283 between overlapping faults where the separation distance exceeds 15% of their total length.
284 Gupta and Scholz (2000) assumed the stress distribution surrounding an isolated normal
285 fault is a first-order approximation of the stress field surrounding two interacting faults (Fig.
286 8). The stress field surrounding a relay zone can in fact be quite perturbed (Segall and
287 Pollard, 1980; Crider and Pollard, 1998), and more complex models that explicitly capture
288 fault growth and/or mechanical interaction are available (Willemse et al., 1996; Crider and

289   Pollard, 1998; Imber et al., 2004). However, this degree of sophistication is not required for
290   our purposes.

291   Gupta and Scholz (2000) considered the shear stress changes induced on a normal fault (F1)
292   by slip on a neighbouring fault (F2; **Error! Reference source not found.**Fig. 8). The stress
293   drop following slip on F2 is calculated from the surface deflection and an assumed slip
294   distribution on the fault surface. An increase in stress at the tip of F2 is assumed in order for
295   the fault to propagate (Fig. 8). For a given fault segment size and material properties of the
296   host rock, there is a critical stress drop contour located within the stress drop region of the
297   adjacent to F2 (Fig. 8), through which an overlapping fault (F1) does not propagate (Gupta
298   and Scholz, 2000). The critical stress drop contour coincides with the boundary of the stress
299   shadow region outlined in (Ackermann and Schlische, 1997). The interaction between the
300   propagating fault tip and the critical stress drop contour limits the overlap of the bounding
301   faults, providing an upper bound on the aspect ratio of the relay ramp. The important point
302   here is that the size of the stress drop zone, and the radius of the critical stress contour,
303   scale with the size of the bounding faults. Thus, the maximum separation and overlap
304   dimensions of any potential relay ramp will increase along with displacement on the
305   bounding faults, but aspect ratios will remain approximately constant.

5.2   Kinematic model to explain the development of individual relay zone geometries

308   The simple model of fault interaction, in section 5.1, can account for the power-law
309   relationship between fault overlap and separation in relay zones. However, it does not
310   explain the variation in relay zone geometry identified in section 4 (Figs. 6 and 7), nor does it
311   account for the order of magnitude scatter observed within the separation and overlap
312   data. In this section, we outline a kinematic model for the 3D geometric evolution of
313   individual relay zones, based on the interaction and linkage of two initially isolated normal
314   faults, which is consistent with Gupta and Scholz (2000). However, the model is not unique.
315   As discussed below, some of the geometries observed in Fig. 7 could arise due to fault
316   surface bifurcation, rather than interaction and linkage of two initially isolated faults.

317   Stage 1 corresponds to the type one relay zones identified in Fig. 6. The characteristic relay

318   ramp geometries within a single Stage 1 relay zone are: low aspect ratios near the upper tip

319   lines, maximum aspect ratios around the centre of the relay zone, and low aspect ratios

320   near the lower tip lines (Figs. 9a and b). Fault separation varies little with depth and is

321   controlled by the original separation distance between the overlapping fault segments (Fig.

322   9a). Maximum overlap occurs towards the centre of the relay zone where displacements on

323   the bounding faults are the highest. At this early stage of relay zone development, the tip

324   lines of the overlapping bounding faults are approximately elliptical in strike projection (Fig.

325   9c). During Stage 1, we suggest that unrestricted, elliptical fault tip lines overlap to form a

326   relay zone (Fig. 9c), resulting in a large spread in fault overlap at different depths within the

327   relay zone (Fig. 9a).

328   During Stage 2, the lateral tip lines of the relay-bounding faults are sub-vertical within the

329   relay zone (Fig. 9b). Overlap length and separation are approximately constant with depth.

330   The separation is equal to that of the original separation distance of the overlapping fault

331   segments (Fig. 9a). Sub-vertical tip lines develop in response to further displacement

332   accumulation and propagation of the relay-bounding faults. As such, sub-vertical lateral tip

333   lines may develop when the relay-bounding faults become pinned and subsequent

334   propagation is retarded (Gupta and Scholz, 2000).

335   During Stage 3, further displacement accumulation on the relay-bounding faults gives rise to

336   linked relay zones. The tip line geometries will depend on the location and extent of fault

337   linkage (Kristensen et al., 2008; Long and Imber, in review). In relay zones that display down-

338   dip fault linkage, along slip-normal branch lines, the separation distance decreases with

339   depth, as fault propagate towards each other (Fig. 9e). This results in an increase in relay

340   zone aspect ratio with depth towards the branch line, if fault overlap length remains the

341   same, such as in Laminaria east R9 (Fig. 6a and b). Alternatively, a downward-decrease in

342   separation between the relay-bounding faults could arise due to fault surface bifurcation,

343   rather than linkage processes (e.g. Childs et al., 1995; Childs et al., 1997; Kristensen et al.,

344   2008).

345   The proposed geometric progression is based on a relay zone consisting of two planar,

346   initially isolated faults (Fig. 9b). However, fault propagation within a heterogeneous layered

347 sequence will inevitably lead to irregular lobed shaped tip lines (Huggins et al., 1995;
348 Marchal et al., 2003; Schöpfer et al., 2006), which become out-of-plane with one another
349 (Childs et al., 1996b) and overlap to form a relay zone. The geometric evolution of relay
350 zones formed by the bifurcation of fault tip lines has already been document (Childs et al.,
351 1995; Huggins et al., 1995; Childs et al., 1997; Kristensen et al., 2008). In such relay zones,
352 the bounding faults are linked at depth throughout the growth of the relay zone and both
353 the overlap and separation may vary with depth at all stages during relay zone
354 development.

5.3   Influence of mechanical stratigraphy and heterogeneity

356 The post-depositional normal faults at Lamberton have maximum displacements of less
357 than 20 cm, and cut and offset an inter-bedded sandstone-shale sequence. Their upper tip
358 lines are restricted by a shale layer (c. 80 cm thick), which overlies this sequence (Long,
359 2011). The post-depositional normal faults at Kilve developed in and offset an interbedded
360 limestone-shale sequence. They nucleated within the mechanically strong limestone beds
361 and were initially confined by intervening shale layers (Peacock and Sanderson, 1992; Crider
362 and Peacock, 2004).

363 Dip-slip faults within mechanically confined sequences are free to propagate laterally but
364 are restricted vertically. This results in long faults with relatively low displacements
365 (Benedicto et al., 2003). The width of the stress shadow zone bounded by the critical stress
366 drop contour relates to the displacement and shape of the fault. Large displacement faults
367 produce wider stress drop regions than small displacement faults (Willemse, 1997; Gupta
368 and Scholz, 2000). Faults that are mechanically confined therefore have relatively narrow
369 stress drop zones for their length (Fig. 10a). In addition, despite increases in fault length, the
370 displacement remains low and therefore the value of the critical stress drop contour is
371 approximately constant (Soliva et al., 2006). Mechanically confined faults with separation
372 distances (Fig. 10b: S*) that are greater than the radius of the critical stress drop contour
373 (Fig. 10b: D*) are able to overlap un-hindered by neighbouring faults as they accommodate
374 extension. The initially confined faults eventually propagate through the confining layer.
375 Displacement now increases and the stress shadow enlarges (i.e. D* increases) (Fig. 10c).
376 Eventually the stress field will grow to a point where the critical stress drop contour will

377   intersect with the overlapping fault tip (Fig. 8), which stops further propagation (Fig. 10d). In

378   this way, the aspect ratios of relay ramps formed between mechanically confined relay-

379   bounding faults are predicted to be greater than those whose growth is unrestricted.

380   The concept behind this proposed model is supported by observations made by Soliva et al.,

381   (2008), who observed elevated aspect ratios for a relay ramp that was bounded by a low

382   displacement footwall fault. The low displacement on the footwall fault resulted from

383   restrictions on slip due to a reduction in fault dip near a slip-normal branch line. The cause

384   of the restricted displacement differs from that inferred from Lamberton, but the underlying

385   relationship between reduced displacement and increased fault overlap length is the same.

386   Faults at Kilve are also closely associated with pre-existing veins, which are oriented sub-

387   parallel to the strike of the faults. The presence of vein material at fault tips could change

388   the yield strength needed to be overcome by a propagating the fault. We postulate that the

389   calcite veins themselves, and/or the vein-wall rock interfaces have lower yield strengths

390   than intact limestone. No yield strength measurements are known to exist for calcite veins,

391   although previous authors suggest that veins are relatively weak structures compared to the

392   intact host rock (Peacock and Sanderson, 1994; Crider and Peacock, 2004). If this is correct,

393   the presence of pre-existing veins may further enhance fault propagation, again giving rise

394   to relay ramps with large aspect ratios.

395   The proposed modifications to Gupta and Scholz's (2000) model of fault interaction are only

396   applicable in situations that have similar controls to Lamberton and Kilve, i.e. mechanical

397   layering that restricts fault growth and/or the presence of pre-existing structures that

398   influence fault tip propagation. Therefore, the scale over which these controls operate

399   depends strongly on the size of the faults relative to the thickness of the mechanical layers

400   or size of heterogeneity. Further research is needed to test whether such controls on relay

401   aspect ratios are applicable to larger scale structures than are observed at Lamberton and

402   Kilve.

6   Conclusions

1. Overlap and separation distances for relay-bounding faults have been measured for 225 relay ramps, using a consistent approach that takes account of both continuous and discontinuous deformation to accurately define relay ramp geometry. A correction factor has been applied to published overlap and separation distances, which have been combined with our new measurements to produce a refined global dataset of relay zone geometries.

2. The refined dataset of overlap and separation distances for relay-bounding faults displays a single power-law scaling trend over nearly 8 orders of magnitude. The best-fit power-law trend line is $y=3.634x^{0.97}$ $R^2=0.98$ and the mean aspect ratio of 4.2 and a standard deviation of 3.0. This conclusion similar to published datasets which have power-law exponents of 0.97 and mean aspect ratios (overlap/separation) between 4 and 4.9. However, at all observed scales there exists an order of magnitude scatter in both overlap and separation.

3. The overall power-law scaling between overlap and separation distance suggests that a single mechanism, common at all scales, controls the first-order geometry of relay zones. It is inferred that stress field interaction of overlapping faults could be the primary controlling factor in relay ramp geometries, as exemplified by the Gupta and Scholz (2000) elastic-plastic model of fault interaction. Host-rock lithology is not a first-order control on relay ramp geometry.

4. Almost all the scatter in the global dataset of relay ramp overlap and separation distances can be accounted for by the variation in 3D geometry within individual relay zones. This variability reflects processes associated with fault surface bifurcation, relay growth and breaching.

5. Specific instances occur where relay ramps have aspect ratios more than twice that of the global mean. Relay ramps with high aspect ratios may develop where growth of the relay-bounding faults is restricted by the mechanical layering, and/or where fault tip propagation is enhanced by the presence of pre-existing structures, such as veins.

7   Acknowledgements

8   Figure list

Fig. 1. (a) A schematic depiction of a relay ramp in map view. Fault overlap is measured between the two overlapping fault tips and separation is the perpendicular distance between the two fault segments measured at the centre of the relay ramp. Relay aspect ratio = Overlap/Separation. (b) A linked relay ramp. Overlap length is measured between the branch point and the fault tip. (c) A fully breached relay ramp. Overlap length is measured between the two branch points. (d) In three-dimensions, faults have a component of heave and the separation distance is thus the distance between the fault polygon centrelines. (e) When a relay ramp is bounded by two laterally continuous monoclines (Long and Imber, 2010), the separation distance is measured between the points of maximum deflection on the limbs of each monocline. (f) Seismic reflection datasets have limited resolution. Laterally continuous monoclines could therefore result from different combinations of sub-seismic scale faults, each with a different location to which separation should be measured (white circle; see text for further explanation).

Fig. 2. A limestone bed exposed at Kilve, Somerset, UK, showing a "simple" relay ramp that resembles the schematic depiction of a relay ramp in Fig. 1a. Fault tips for faults F1 and F2 are annotated T1 and T2, respectively. Veins are located along-strike of the fault tips, annotated V1 and V2, respectively. (b) A schematic displacement-distance plot for faults F1 and F2 (a). Fault tips are located at the point where the measureable displacement on the fault decreases to zero.

Fig. 3. (a) Cross-section view of a monocline from Kilve. Rotation of the limestone beds is accommodated by veining and minor fault movement. (b) Map showing the distribution of continuous deformation (i.e. monoclinal folding) at the tip of the fault. (Apparent) dips have been measured on transect lines oriented perpendicular to the axis of the monocline. Map is derived from terrestrial laser scans of the Kilve foreshore. (c) Vertical displacement (throw) vs. distance plot along the axis of the monocline. Displacements have been calculated from the apparent dips shown in (b). Displacement decreases steadily towards the west. The west end of the monocline is covered by sand. (d) A displacement-distance plot with fault throw recorded from the field and displacements measured across the monocline (b and c). Despite the change from fault to monocline, displacement decreases continuously towards the west.

Fig. 4. Aspect ratio plotted against depth for a single relay zone from the Inner Moray Firth, mapped using 3D seismic data. For the light grey profile, relay overlap and separation are measured using only discontinuous fault offsets, i.e. fault polygons. The black profile includes the regions of continuous, coherent deformation around the mapped faults in measurements of relay aspect ratio. The difference in measured aspect ratio between the two profiles is approximately 1.1 for each horizon. The largest aspect ratios are found towards the centre of the relay zone; the upper section of the relay zone (above 170 ms TWT) has elevated aspect ratios compared to the lower section of the relay (below 2000 ms).

Fig. 5. (a) Log-log plot of relay overlap verses separation for data collected in this study (circles) and from literature sources (diamonds). Literature sources used in this plot are listed in the Supplementary Material: Relay table 2. (b) Measurement of relay zone overlap and separation before and after continuous deformation was included. Relay zones from a range of scales are plotted (IMF R1 and Laminaria east R7). Including continuous deformation in the measurement of relay aspect ratios increases measurements by a near constant factor. (c) Corrected literature data to take into account the potential under-sampling of fault overlap when continuous deformation is not included, as seen in (b). In general, over 8 orders of magnitude there is approximately an equal amount of scatter of measurements about a single power-law trend. (d) Relay measurements are coloured for lithology. There is no systematic relationship between lithology and relay zone aspect ratio.

Fig. 6. (a) Log-log plot of overlap verses separation for individual relay zones (large symbols). Data for each relay zone have been circled to highlight trends in the spread of data. Three trends are recognised: sub-vertical distributions (dashed black line), point distributions (solid grey line), and horizontal distributions (solid black line). The range of aspect ratios measured from individual relay zones span almost the entire scatter in the global dataset (grey dots). (b) Relay aspect ratio against normalised depth, in order to show changes in aspect ratio between the top and bottom of relay zones. Details on each location can be found in Supplementary Material: Relay table. 1. As in (a) three trends are recognised; low-high-low vertical aspect ratio profiles (dashed black line), approximately uniform aspect ratio with depth (solid grey line), low-high vertical aspect ratio profiles (solid black line). Relay zones Laminaria east R8, R6, R7 and west R2 display modified vertical aspect ratio profiles, see (Fig. 7).

Fig. 7. Perspective 3D images of mapped "true" tip line geometries (solid black lines), branch lines (thick solid black lines), branch points (black circles), and horizon-fault intersections (dashed lines). The "true" tip line locations include the fault-related continuous deformation (see section 2). (a) Type 1 example: IMF R1. (b) Type 2 example: Laminaria east R1. (c) Type 3 example: Laminaria east R9. (d) An example of a relay zone that does not conform to idealised geometries. Relay Laminaria east R7.

Fig. 8. Map view of the stress field around fault F2 and its interaction with the propagating tip of F1. The stress field for F2 is modelled as if it were an isolated fault, which is taken to be a first order approximation of the stress field for the relay zone. Each fault is surrounded by a region of stress drop in the footwall and hanging wall, and stress increase near the tips. Taken from Gupta and Scholz, (2000).

Fig. 9. The three stages in the geometric evolution of a relay zone, identified from Fig. 6. (a) The schematic changes in overlap and separation for each relay zone, circled. Stage 1, the relay zone has a large spread in overlap length compared to separation. Stage 2, separation remains the same as in stage 1, but overlap length at all levels within the relay zone are now similar. Stage 3, overlap length remains similar to stage 2, whereas separation now decreases within the relay zone. (b) AR plotted against depth for each stage of relay zone development. (c-e) 3D schematic models of the geometry of the relay zones at the three

stages in their evolution. (c) Stage 1, the relay zone is bounded by faults with upward/downward retreating tip lines which results in a high degree of scatter in overlap length, but not separation. Separation is set by the original location of the bounding faults. (d) Stage 2, the bounding faults are laterally pinned by the adjacent fault and develop sub-vertical tip lines. (e) Stage 3, breaching of a relay zone occurs when faults propagate towards each other and link, which results in a decrease in fault separation at certain levels within the relay zone.

Fig. 10. A modification to Gupta and Scholz, (2000) fault interaction model based on observations from Lamberton. The model includes a fault array that is initially confined within a mechanical layer. (a) Faults initiate within a strong mechanical layer. (b) The faults are confined within the mechanical layer and develop low displacement-length ratios, with relatively small stress fields when compared to unconfined faults with similar lengths. D* is the maximum distance of the critical stress drop contour from the fault trace. S* is the separation distance between two overlapping faults. (c) Faults begin to propagate through the mechanical layer into surrounding strata. The size of the stress shadows grow as fault displacement increases. At a certain point the critical stress drop contour will interact with the nearby fault tip, preventing further overlap. (d) Fault linkage occurs and a through going fault is formed. Large aspect ratios are produced by accumulating large overlap lengths in stage (b) prior to the expansion of the stress fields in (c). Figure style after (Soliva et al., 2006: their Fig. 14).

9　　References

Ackermann, R.V., Schlische, R.W., 1997. Anticlustering of small normal faults around larger faults. Geology 25 (12), 1127-1130.

Acocella, V., Gudmundsson, A., Funiciello, R., 2000. Interaction and linkage of extension fractures and normal faults: examples from the rift zone of Iceland. Journal of Structural Geology 22 (9), 1233-1246.

Anders, M.H., Schlische, R.W., 1994. Overlapping Faults, Intrabasin Highs, and the Growth of Normal Faults. The Journal of Geology 102 (2), 165-179.

548 Aydin, A., Schultz, R.A., 1990. Effect of mechanical interaction on the development of strike-
549   slip faults with echelon patterns. Journal of Structural Geology 12 (1), 123-129.

550 Barnett, J., Mortimer, J., Rippon, J., Walsh, J., Watterson, J., 1987. Displacement geometry in
551   the volume containing a single normal fault. AAPG Bulletin 71 (8), 925-937.

552 Benedicto, A., Schultz, R.A., Soliva, R., 2003. Layer thickness and the shape of faults.
553   Geophys. Res. Lett. 30 (20), 2076.

554 Cartwright, J., 1991. The kinematic evolution of the Coffee Soil Fault. Geological Society,
555   London, Special Publications 56 (1), 29-40.

556 Cartwright, J., Mansfield, C., Trudgill, B., 1996. The growth of normal faults by segment
557   linkage, In: Buchanan, P.G., Nieuwland, D.A. (Eds.), Modern developments in
558   structural interpretation. Geological Society, London, Special Publications pp. 163-
559   177.

560 Childs, C., Nicol, A., Walsh, J.J., Watterson, J., 1996a. Growth of vertically segmented normal
561   faults. Journal of Structural Geology 18 (12), 1389-1397.

562 Childs, C., Walsh, J.J., Watterson, J., 1997. Complexity in fault zone structure and
563   implications for fault seal prediction, In: P. Møller-Pedersen, D., A.G. Koestler, D.
564   (Eds.), Norwegian Petroleum Society Special Publications. Elsevier, pp. 61-72.

565 Childs, C., Watterson, J., Walsh, J.J., 1995. Fault overlap zones within developing normal
566   fault systems. Journal of the Geological Society of London 152 (3), 535-549.

567 Childs, C., Watterson, J., Walsh, J.J., 1996b. A model for the structure and development of
568   fault zones. Journal of the Geological Society of London 153 (3), 337-340.

569 Cowie, P.A., Roberts, G.P., 2001. Constraining slip rates and spacings for active normal
570   faults. Journal of Structural Geology 23 (12), 1901-1915.

571 Crider, J., Pollard, D., 1998. Fault linkage: Three-dimensional mechanical interaction
572   between echelon normal faults. Journal of Geophysical Research 103 (B10), 24373-
573   24391.

574 Crider, J.G., Peacock, D.C.P., 2004. Initiation of brittle faults in the upper crust: a review of
575   field observations. Journal of Structural Geology 26 (4), 691-707.

576 Ferrill, D.A., Morris, A.P., 2008. Fault zone deformation controlled by carbonate mechanical
577   stratigraphy, Balcones fault system, Texas. AAPG Bulletin 92 (3), 359-380.

578 Gawthorpe, R.L., Hurst, J.M., 1993. Transfer zones in extensional basins: their structural
579   style and influence on drainage development and stratigraphy. Journal of the
580   Geological Society 150 (6), 1137-1152.

581 Gupta, A., Scholz, C.H., 1998. Utility of elastic models in predicting fault displacement fields.
582   J. Geophys. Res. 103 (B1), 823-834.

583 Gupta, A., Scholz, C.H., 2000. A model of normal fault interaction based on observations and
584   theory. Journal of Structural Geology 22 (7), 865-879.

585 Huggins, P., Watterson, J., Walsh, J.J., Childs, C., 1995. Relay zone geometry and
586   displacement transfer between normal faults recorded in coal-mine plans. Journal of
587   Structural Geology 17 (12), 1741-1755.

588 Imber, J., Tuckwell, G.W., Childs, C., Walsh, J.J., Manzocchi, T., Heath, A.E., Bonson, C.G.,
589   Strand, J., 2004. Three-dimensional distinct element modelling of relay growth and
590   breaching along normal faults. Journal of Structural Geology 26 (10), 1897-1911.

591 Kristensen, M.B., Childs, C.J., Korstgård, J.A., 2008. The 3D geometry of small-scale relay
592   zones between normal faults in soft sediments. Journal of Structural Geology 30 (2),
593   257-272.

594 Larsen, P.-H., 1988. Relay structures in a Lower Permian basement-involved extension
595   system, East Greenland. Journal of Structural Geology 10 (1), 3-8.

596 Long, J.J., 2011. Geometry, evolution and scaling of fault relay zones in 3D using detailed
597   observations from outcrops and 3D seismic data. Ph.D. Thesis, Durham University.

598 Long, J.J., Imber, J., 2010. Geometrically coherent continuous deformation in the volume
599   surrounding a seismically imaged normal fault-array. Journal of Structural Geology
600   32 (2), 222-234.

601 Long, J.J., Imber, J., in review. Strain compatibility and fault linkage evolution in relay zones
602   on normal faults. Journal of Structural Geology.

603 Marchal, D., Guiraud, M., Rives, T., 2003. Geometric and morphologic evolution of normal
604   fault planes and traces from 2D to 4D data. Journal of Structural Geology 25 (1), 135-
605   158.

606 McLeod, A.E., Dawers, N.H., Underhill, J.R., 2000. The propagation and linkage of normal
607   faults: insights from the Strathspey-Brent-Statfjord fault array, northern North Sea.
608   Basin Research 12 (3-4), 263-284.

609   Morley, C.K., 2002. Evolution of Large Normal Faults: Evidence from Seismic Reflection Data.
610   AAPG Bulletin 86 (6), 961-978.

611   Morley, C.K., Nelson, R.A., Patton, T.L., Munn, S.G., 1990. Transfer zones in the East African
612   Rift system and their relevance to hydrocarbon exploration in rifts. AAPG Bulletin 74
613   (8), 1234-1253.

614   Peacock, D.C.P., 2002. Propagation, interaction and linkage in normal fault systems. Earth-
615   Science Reviews 58 (1-2), 121-142.

616   Peacock, D.C.P., Parfitt, E.A., Wilkerson, M.S., Fischer, M.P., Apotria, T., 2002. Active relay
617   ramps and normal fault propagation on Kilauea Volcano, Hawaii. Journal of
618   Structural Geology 24729-742.

619   Peacock, D.C.P., Price, S.P., Whitham, A.G., Pickles, C.S., 2000. The world's biggest relay
620   ramp; Hold With Hope, NE Greenland. Journal of Structural Geology 22 (7), 843-850.

621   Peacock, D.C.P., Sanderson, D.J., 1991. Displacements, segment linkage and relay ramps in
622   normal fault zones. Journal of Structural Geology 13 (6), 721-733.

623   Peacock, D.C.P., Sanderson, D.J., 1992. Effects of layering and anisotropy on fault geometry.
624   Journal of the Geological Society 149 (5), 793-802.

625   Peacock, D.C.P., Sanderson, D.J., 1994. Geometry and development of relay ramps in normal
626   fault systems. AAPG Bulletin 78 (2), 147-165.

627   Roberts, S., Jackson, J., 1991. Active normal faulting in central Greece: an overview.
628   Geological Society, London, Special Publications 56 (1), 125-142.

629   Schöpfer, M.P.J., Childs, C., Walsh, J.J., 2006. Localisation of normal faults in multilayer
630   sequences. Journal of Structural Geology 28 (5), 816-833.

631   Segall, P., Pollard, D.D., 1980. Mechanics of Discontinuous Faults. J. Geophys. Res. 85 (B8),
632   4337-4350.

633   Soliva, R., Benedicto, A., 2004. A linkage criterion for segmented normal faults. Journal of
634   Structural Geology 26 (12), 2251-2267.

635   Soliva, R., Benedicto, A., Maerten, L., 2006. Spacing and linkage of confined normal faults:
636   Importance of mechanical thickness. Journal of Geophysical Research 111 (B1).

637   Soliva, R., Benedicto, A., Schultz, R.A., Maerten, L., Micarelli, L., 2008. Displacement and
638   interaction of normal fault segments branched at depth: Implications for fault
639   growth and potential earthquake rupture size. Journal of Structural Geology 30 (10),
640   1288-1299.

641   Steen, O., Sverdrup, E., Hanssen, T.H., 1998. Predicting the distribution of small faults in a
642   hydrocarbon reservoir by combining outcrop, seismic and well data, In: Jones, G.,
643   Fisher, Q.J., Knipe, R.J. (Eds.), Faulting, fault sealing and fluid flow in hydrocarbon
644   reservoirs. Geological Society Special Publication, London, pp. 27-50.

645   Stewart, I.S., Hancock, P.L., 1991. Scales of structural heterogeneity within neotectonic
646   normal fault zones in the Aegean region. Journal of Structural Geology 13 (2), 191-
647   204.

648   Townsend, C., Firth, I., Westerman, R., Kirkevollen, L., Harde, M., Andersen, T., 1998. Small
649   seismic-scale fault identification and mapping, In: Jones, G., Fisher, Q.J., Knipe, R.J.
650   (Eds.), Faulting, fault sealing and fluid flow in hydrocarbon reservoirs. Geological
651   Society, London, Special Publications, pp. 1-25.

652   Trudgill, B., Cartwright, J., 1994. Relay-ramp forms and normal-fault linkages, Canyonlands
653   National Park, Utah. Geological Society of America Bulletin 106 (9), 1143.

654   Walsh, J.J., Bailey, W.R., Childs, C., Nicol, A., Bonson, C.G., 2003. Formation of segmented
655   normal faults; a 3-D perspective. Journal of Structural Geology 25 (8), 1251-1262.

656   Walsh, J.J., Watterson, J., 1991. Geometric and kinematic coherence and scale effects in
657   normal fault systems, In: Roberts, A.M., Yielding, G., Freeman, B. (Eds.), The
658   geometry of normal faults. Geological Society, London, Special Publications, pp. 193-
659   203.

660   Walsh, J.J., Watterson, J., Bailey, W.R., Childs, C., 1999. Fault relays, bends and branch-lines.
661   Journal of Structural Geology 21 (8-9), 1019-1026.

662   Walsh, J.J., Watterson, J., Childs, C., Nicol, A., 1996. Ductile strain effects in the analysis of
663   seismic interpretations of normal fault systems, In: Buchanan, P.G., Nieuwland, D.A.
664   (Eds.), Modern developments in structural interpretation, validation and modelling.
665   Geological Society Special Publications, pp. 27-40.

666   White, I.R., Crider, J.G., 2006. Extensional fault-propagation folds: mechanical models and
667   observations from the Modoc Plateau, northeastern California. Journal of Structural
668   Geology 28 (7), 1352-1370.

669   Willemse, E.J.M., 1997. Segmented normal faults: Correspondence between three-
670   dimensional mechanical models and field data. J. Geophys. Res. 102 (B1), 675-692.

671   Willemse, E.J.M., Pollard, D.D., Aydin, A., 1996. Three-dimensional analyses of slip

672   distributions on normal fault arrays with consequences for fault scaling. Journal of

673   Structural Geology 18 (2-3), 295-309.

674

675

676

677   Fig.1

678

679

680   Fig. 2

681

Fig. 3

685

686   Fig. 4

687

688

689   Fig. 5

690

a

691

692   Fig. 6

693

694

Fig. 7

696

Fig. 8

697

698

699

a

Relay overlap

Stage 3

Stage 2

Stage 1

Relay separation

b

Aspect ratio

Depth within a relay zone

Stage 1

Stage 3

Stage 2

c

Stage 1

Tip lines

Fault polygons

d

Stage 2

e

Stage 3

Branch lines

700

701   Fig. 9

702
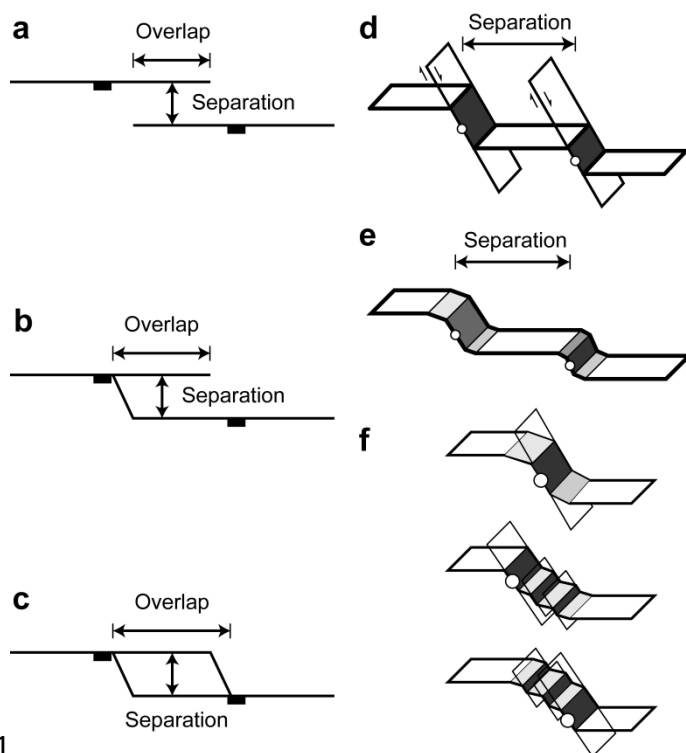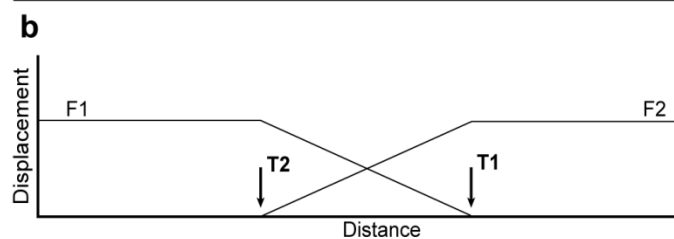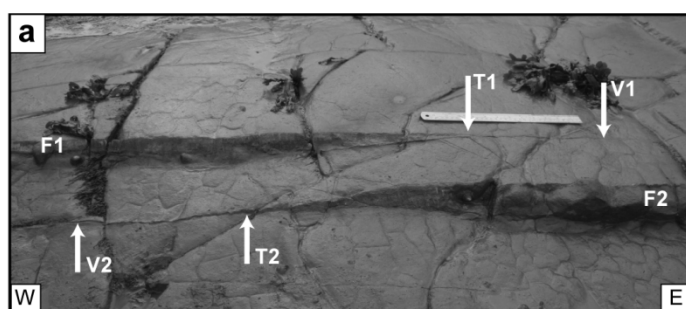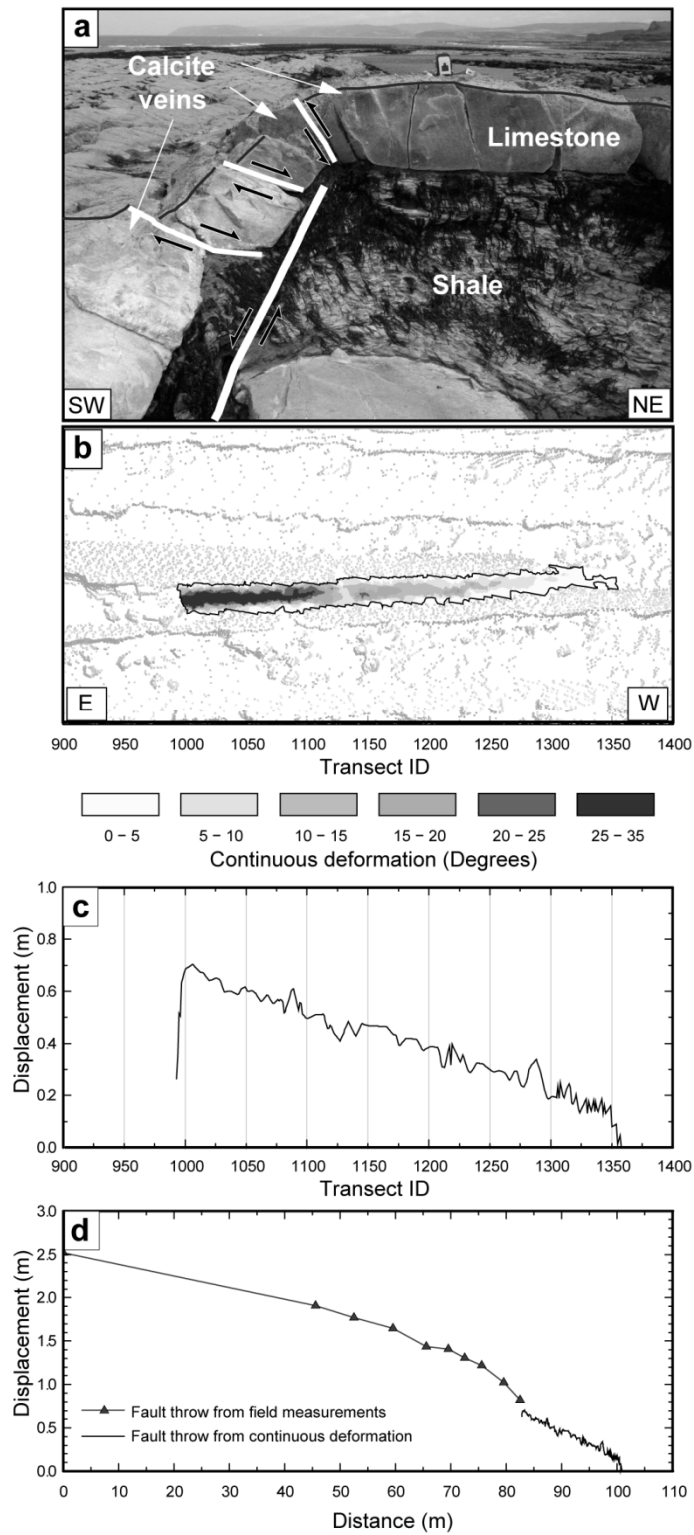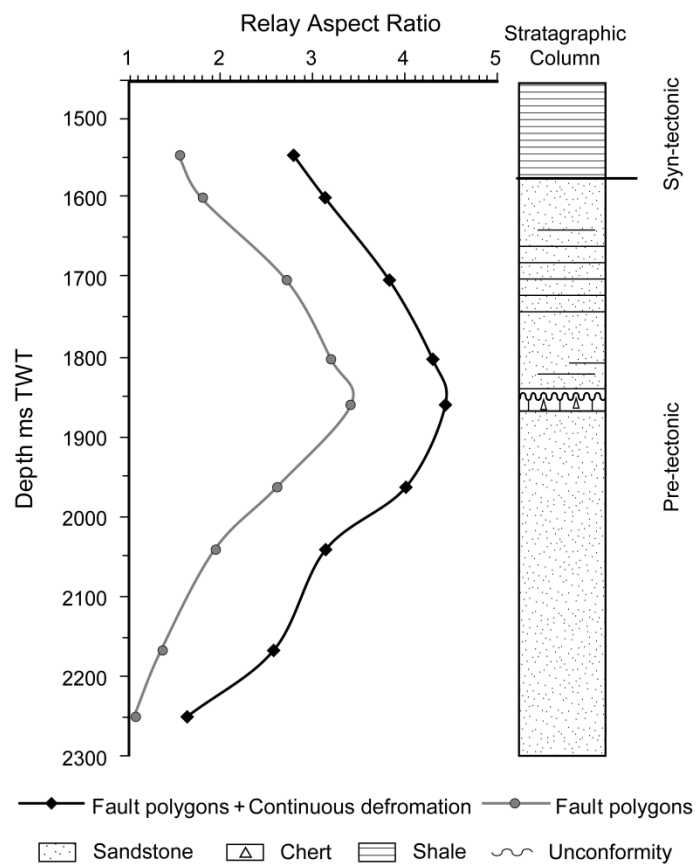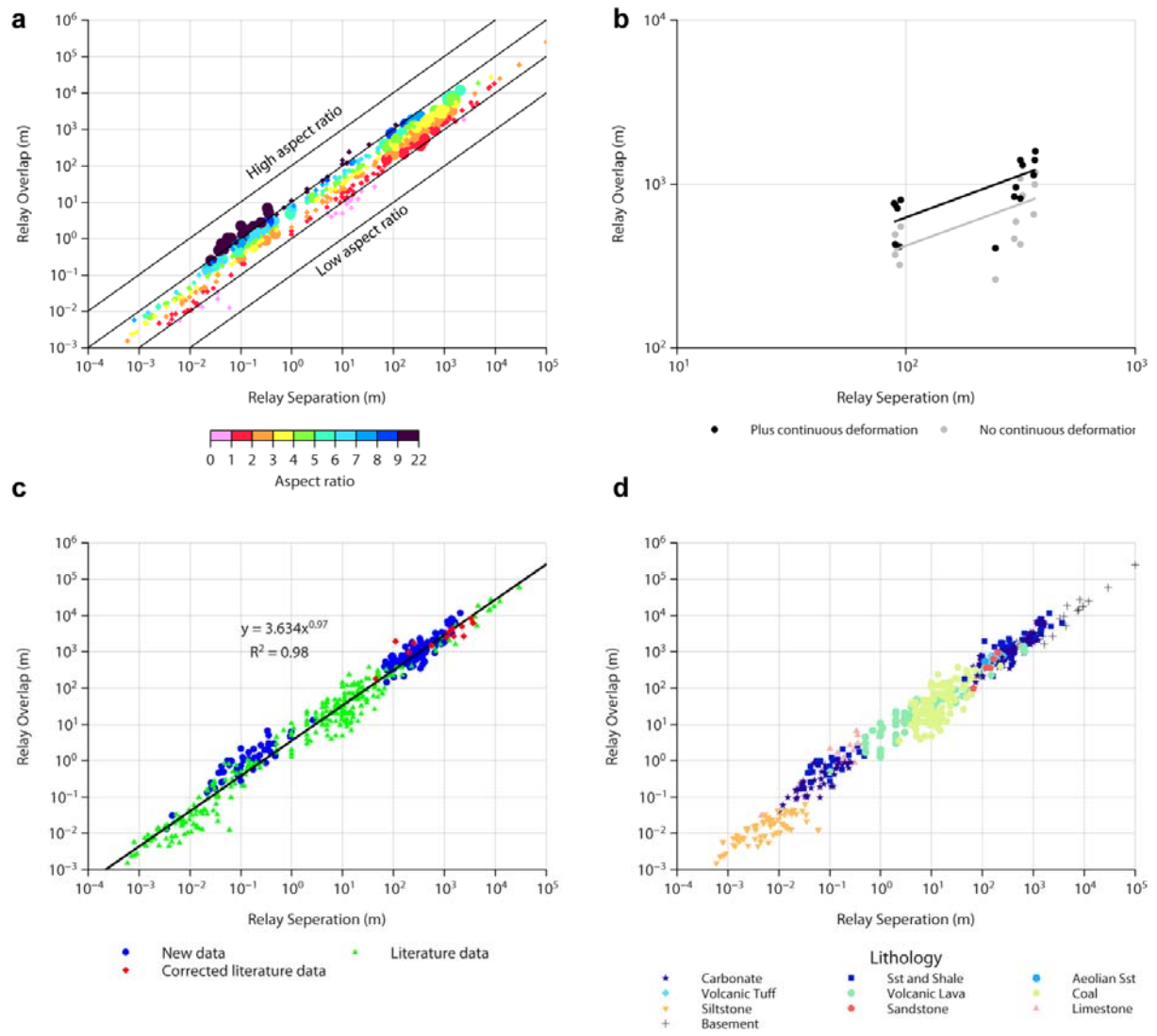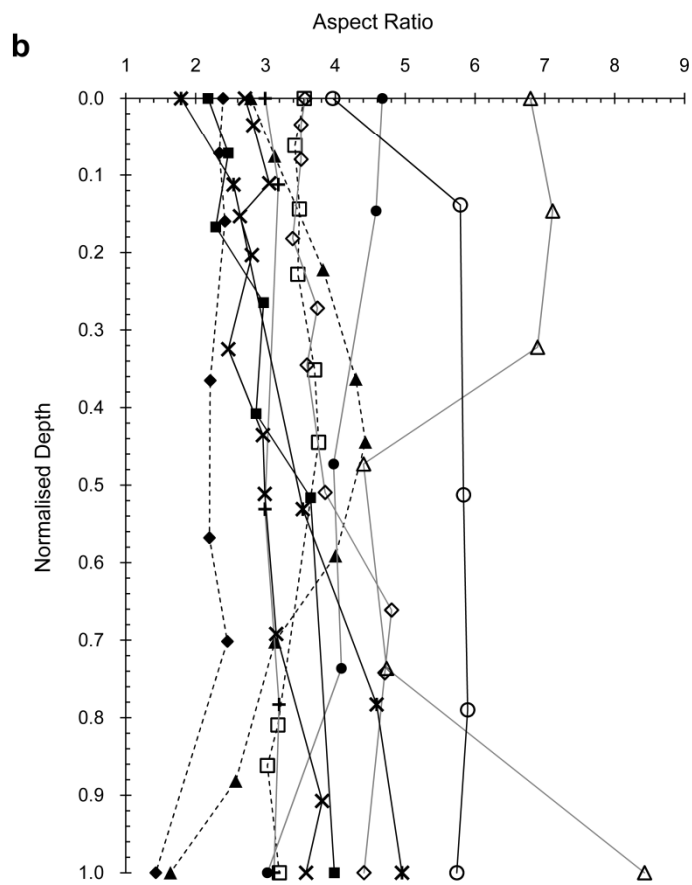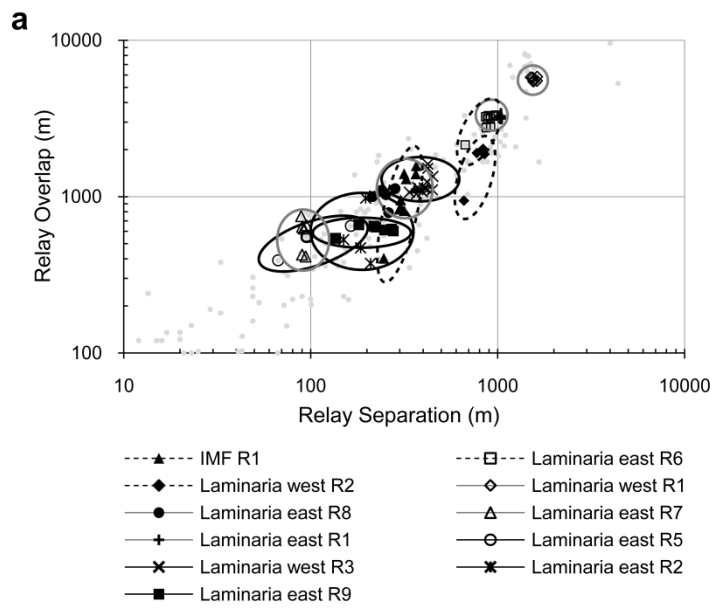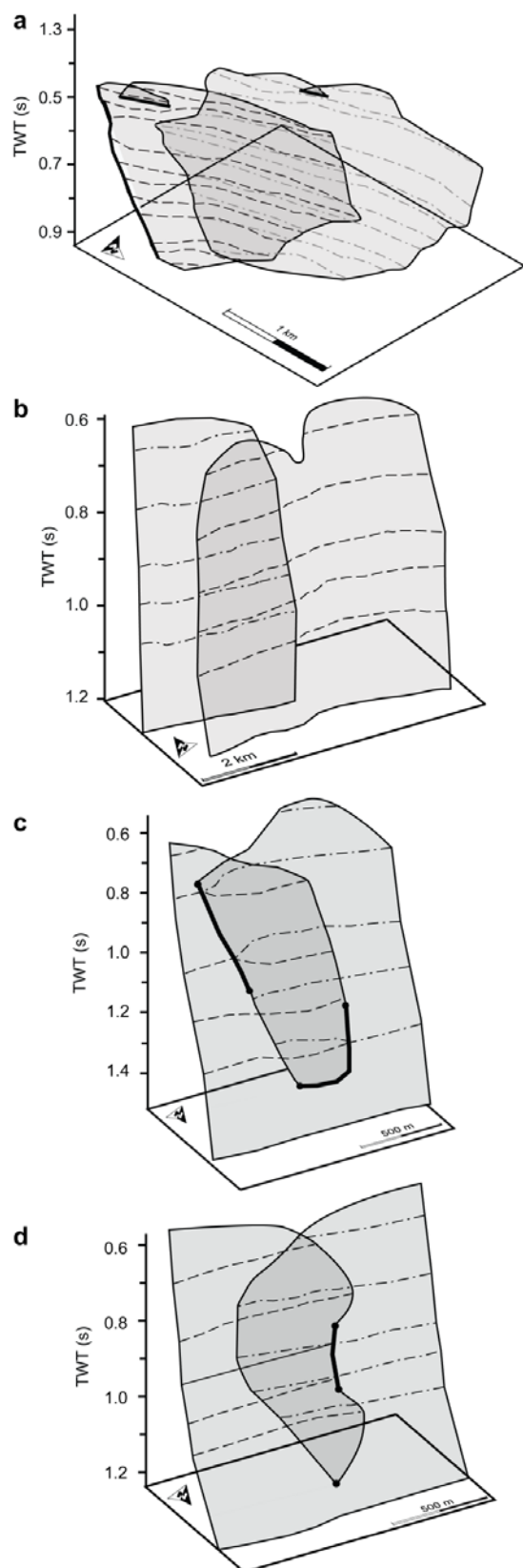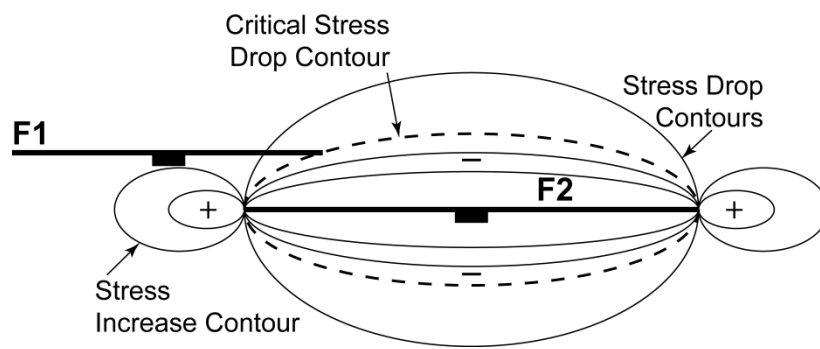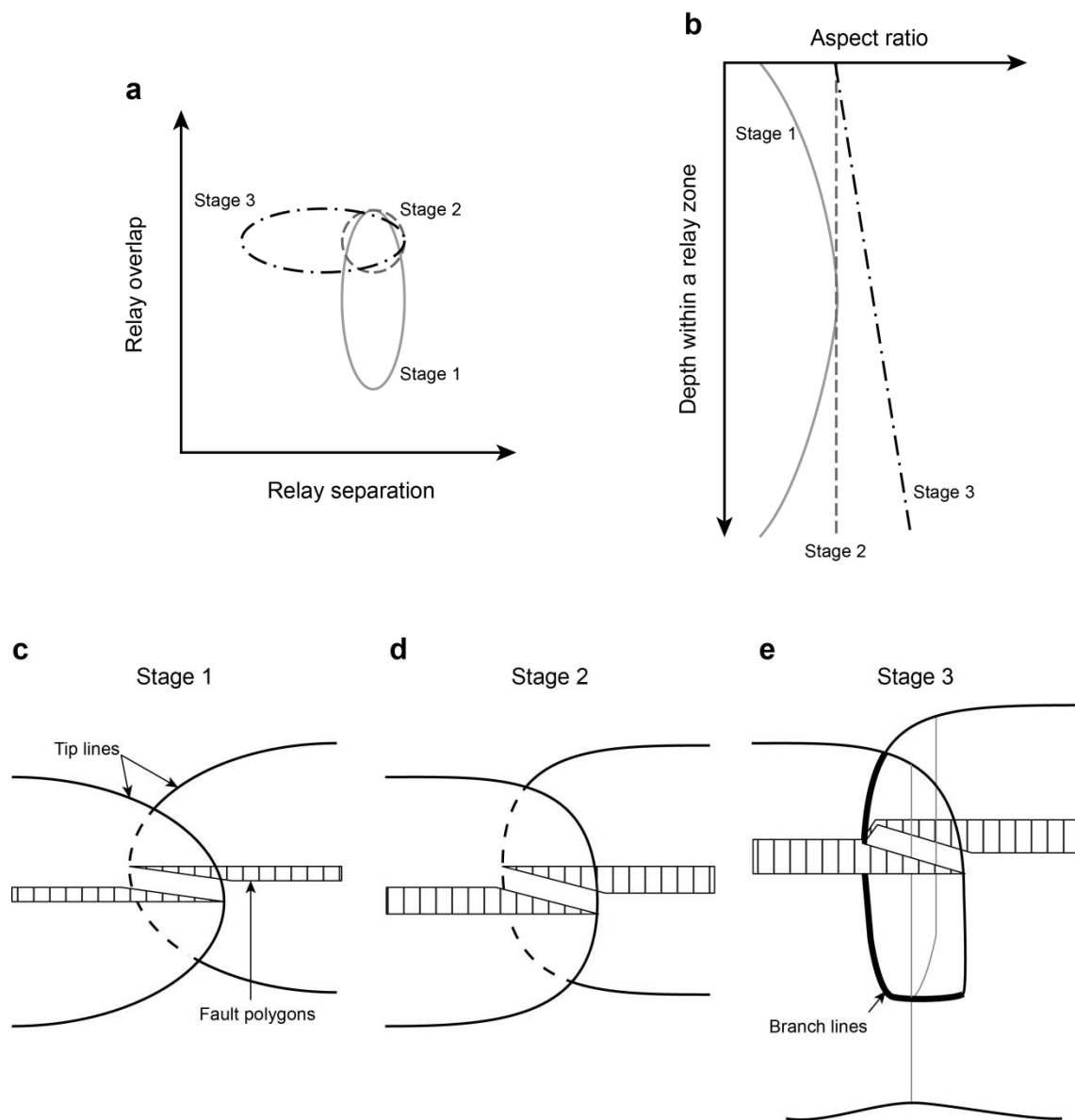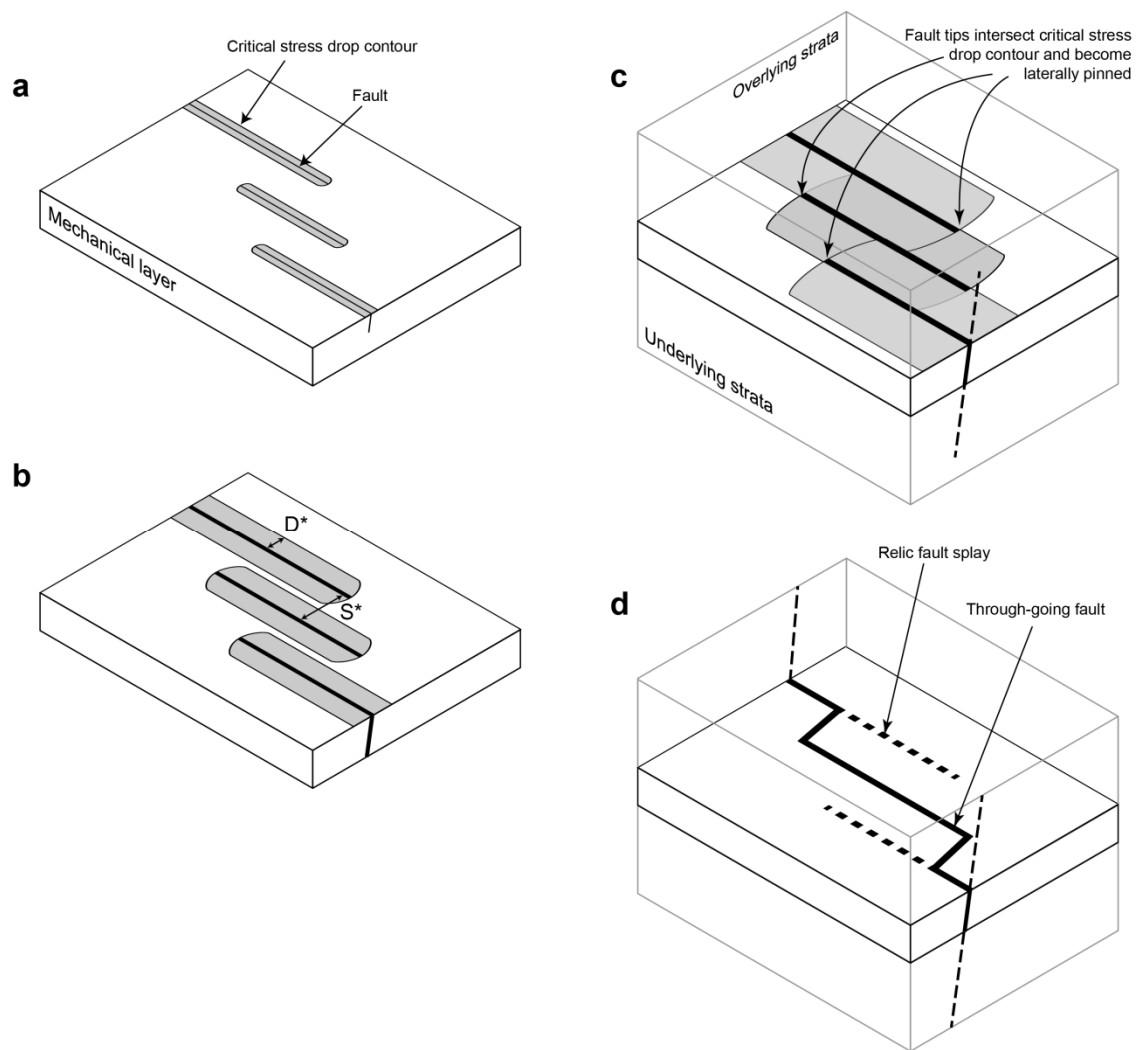
703

704   Fig. 10

705

Digital Appendix

Table: 1. All original relay zone measurements collected during the course of this study.
The first three columns record the geographical locations of individual relay zone measurements.

| Location	Horizon	Relay Ref.	Separation (m)	Overlap (m)	AR	Rock Type(s)	Fault Linkage	Data Type
Lamberton, UK	sst	F_R1	0.1	0.275	2.8	Sst & Shale	Open	Fieldwork
Lamberton, UK	sst	F_R2	0.042	0.252	6.0	Sst & Shale	Linked	Fieldwork
Lamberton, UK	sst	F_R3	0.044	0.268	6.1	Sst & Shale	Linked	Fieldwork
Lamberton, UK	sst	F_R4	0.04	0.488	12.2	Sst & Shale	Linked	Fieldwork
Lamberton, UK	sst	F_R5	0.096	0.578	6.0	Sst & Shale	Linked	Fieldwork
Lamberton, UK	sst	F_R6	0.11	1.243	11.3	Sst & Shale	Linked	Fieldwork
Lamberton, UK	sst	F_R8	0.056	0.936	16.7	Sst & Shale	Linked	Fieldwork
Lamberton, UK	sst	F_R9	0.031	0.174	5.6	Sst & Shale	Fully breached	Fieldwork
Lamberton, UK	sst	F_R10	0.066	0.97	14.7	Sst & Shale	Linked	Fieldwork
Lamberton, UK	sst	F_R11	0.026	0.165	6.3	Sst & Shale	Linked	Fieldwork
Lamberton, UK	sst	F_R12	0.037	0.46	12.4	Sst & Shale	Linked	Fieldwork
Lamberton, UK	sst	F_R13	0.114	1.03	9.0	Sst & Shale	Linked	Fieldwork
Lamberton, UK	sst	F_R14	0.042	0.7	16.7	Sst & Shale	Fully breached	Fieldwork
Lamberton, UK	sst	F_R15	0.098	0.41	4.2	Sst & Shale	Linked	Fieldwork
Lamberton, UK	sst	F_R16	0.064	0.996	15.6	Sst & Shale	Fully breached	Fieldwork
Lamberton, UK	sst	F_R17	0.084	0.606	7.2	Sst & Shale	Linked	Fieldwork
Lamberton, UK	sst	F_R18	0.48	1.33	2.8	Sst & Shale	Open	Fieldwork
Lamberton, UK	sst	F_R19	0.22	0.96	4.4	Sst & Shale	Linked	Fieldwork
Lamberton, UK	sst	F_R20	0.237	1.44	6.1	Sst & Shale	Linked	Fieldwork
Lamberton, UK	sst	F_R21	0.087	0.46	5.3	Sst & Shale	Linked	Fieldwork
Lamberton, UK	sst	F_R22	0.101285714	0.731571429	7.2	Sst & Shale	Linked	Fieldwork
Lamberton, UK	sst_c	R1	0.38	1.7851	4.7	Sst & Shale	Open	Scan
Lamberton, UK	sst_c	R2	0.357	2.611	7.3	Sst & Shale	Linked	Scan
Lamberton, UK	sst_c	R3	0.176	0.577	3.3	Sst & Shale	Fully breached	Scan
Lamberton, UK	sst_c	R4	0.046	0.5	10.9	Sst & Shale	Linked	Scan
Lamberton, UK	sst_c	R5	0.086	0.4	4.7	Sst & Shale	Linked	Scan
Lamberton, UK	sst_c	R6	0.179	2.079	11.6	Sst & Shale	Fully breached	Scan
Lamberton, UK	sst_c	R7	0.0558	1.002	18.0	Sst & Shale	Linked	Scan
Lamberton, UK	sst_c	R8	0.06	0.752	12.5	Sst & Shale	Fully breached	Scan
Lamberton, UK	sst_c	R9	0.145	1.129	7.8	Sst & Shale	Fully breached	Scan

Digital Appendix

Table: 2. Relay zone measurements reproduced from different literature sources.

Location	Separation (m)	Overlap (m)	AR	Corrected Overlap (m)	Corrected AR	Rock Type(s)	Fault Linkage	Data Type	Data Sources
Iceland	150	230	1.5		0.0	Volcanic Lava	-	Fieldwork	Acocella et al. 2000
Iceland	150	380	2.5		0.0	Volcanic Lava	-	Fieldwork	Acocella et al. 2000
Iceland	110	360	3.3		0.0	Volcanic Lava	-	Fieldwork	Acocella et al. 2000
Iceland	90	230	2.6		0.0	Volcanic Lava	-	Fieldwork	Acocella et al. 2000
Iceland	60	70	1.2		0.0	Volcanic Lava	-	Fieldwork	Acocella et al. 2000
Iceland	52	90	1.7		0.0	Volcanic Lava	-	Fieldwork	Acocella et al. 2000
Iceland	40	60	1.5		0.0	Volcanic Lava	-	Fieldwork	Acocella et al. 2000
Iceland	30	40	1.3		0.0	Volcanic Lava	-	Fieldwork	Acocella et al. 2000
Iceland	30	50	1.7		0.0	Volcanic Lava	-	Fieldwork	Acocella et al. 2000
Iceland	30	90	3.0		0.0	Volcanic Lava	-	Fieldwork	Acocella et al. 2000
Iceland	20	60	3.0		0.0	Volcanic Lava	-	Fieldwork	Acocella et al. 2000
Iceland	20	80	4.0		0.0	Volcanic Lava	-	Fieldwork	Acocella et al. 2000
Iceland	18	50	2.8		0.0	Volcanic Lava	-	Fieldwork	Acocella et al. 2000
Iceland	14	50	3.6		0.0	Volcanic Lava	-	Fieldwork	Acocella et al. 2000
Iceland	13	20	1.5		0.0	Volcanic Lava	-	Fieldwork	Acocella et al. 2000
Iceland	12	40	3.3		0.0	Volcanic Lava	-	Fieldwork	Acocella et al. 2000
Iceland	11	43	3.9		0.0	Volcanic Lava	-	Fieldwork	Acocella et al. 2000
Iceland	11	33	3.0		0.0	Volcanic Lava	-	Fieldwork	Acocella et al. 2000
Iceland	10	20	2.0		0.0	Volcanic Lava	-	Fieldwork	Acocella et al. 2000
Iceland	8	20	2.5		0.0	Volcanic Lava	-	Fieldwork	Acocella et al. 2000
Iceland	8	40	5.0		0.0	Volcanic Lava	-	Fieldwork	Acocella et al. 2000
Iceland	7	47	6.7		0.0	Volcanic Lava	-	Fieldwork	Acocella et al. 2000
Iceland	5	14	2.8		0.0	Volcanic Lava	-	Fieldwork	Acocella et al. 2000
Iceland	5	40	8.0		0.0	Volcanic Lava	-	Fieldwork	Acocella et al. 2000
Iceland	5	50	10.0		0.0	Volcanic Lava	-	Fieldwork	Acocella et al. 2000
Iceland	4	9.9	2.5		0.0	Volcanic Lava	-	Fieldwork	Acocella et al. 2000
Iceland	4	11	2.8		0.0	Volcanic Lava	-	Fieldwork	Acocella et al. 2000
Iceland	4	16	4.0		0.0	Volcanic Lava	-	Fieldwork	Acocella et al. 2000
Iceland	4	20	5.0		0.0	Volcanic Lava	-	Fieldwork	Acocella et al. 2000
Iceland	4	30	7.5		0.0	Volcanic Lava	-	Fieldwork	Acocella et al. 2000
Iceland	3.3	13	3.9		0.0	Volcanic Lava	-	Fieldwork	Acocella et al. 2000
Iceland	3	6	2.0		0.0	Volcanic Lava	-	Fieldwork	Acocella et al. 2000
Iceland	3	11	3.7		0.0	Volcanic Lava	-	Fieldwork	Acocella et al. 2000
Iceland	3	16	5.3		0.0	Volcanic Lava	-	Fieldwork	Acocella et al. 2000
Iceland	3	21	7.0		0.0	Volcanic Lava	-	Fieldwork	Acocella et al. 2000
Iceland	2	3	1.5		0.0	Volcanic Lava	-	Fieldwork	Acocella et al. 2000
Iceland	2	4	2.0		0.0	Volcanic Lava	-	Fieldwork	Acocella et al. 2000
Iceland	2	5.3	2.7		0.0	Volcanic Lava	-	Fieldwork	Acocella et al. 2000
Iceland	2	10	5.0		0.0	Volcanic Lava	-	Fieldwork	Acocella et al. 2000
Iceland	2	11	5.5		0.0	Volcanic Lava	-	Fieldwork	Acocella et al. 2000
Iceland	2	13	6.5		0.0	Volcanic Lava	-	Fieldwork	Acocella et al. 2000
Iceland	2	19	9.5		0.0	Volcanic Lava	-	Fieldwork	Acocella et al. 2000
Iceland	2	23	11.5		0.0	Volcanic Lava	-	Fieldwork	Acocella et al. 2000
Iceland	1.1	8	7.3		0.0	Volcanic Lava	-	Fieldwork	Acocella et al. 2000
Iceland	1	1.3	1.3		0.0	Volcanic Lava	-	Fieldwork	Acocella et al. 2000
Iceland	1	1.6	1.6		0.0	Volcanic Lava	-	Fieldwork	Acocella et al. 2000
Iceland	1	2	2.0		0.0	Volcanic Lava	-	Fieldwork	Acocella et al. 2000
Iceland	1	5	5.0		0.0	Volcanic Lava	-	Fieldwork	Acocella et al. 2000
Iceland	1	6	6.0		0.0	Volcanic Lava	-	Fieldwork	Acocella et al. 2000
Iceland	1	11	11.0		0.0	Volcanic Lava	-	Fieldwork	Acocella et al. 2000
Iceland	0.7	7	10.0		0.0	Volcanic Lava	-	Fieldwork	Acocella et al. 2000
Iceland	0.5	2	4.0		0.0	Volcanic Lava	-	Fieldwork	Acocella et al. 2000
Iceland	0.5	1.7	3.4		0.0	Volcanic Lava	-	Fieldwork	Acocella et al. 2000
Iceland	0.5	3	6.0		0.0	Volcanic Lava	-	Fieldwork	Acocella et al. 2000
Iceland	0.5	4.5	9.0		0.0	Volcanic Lava	-	Fieldwork	Acocella et al. 2000
Iceland	0.1	0.5	5.0		0.0	Volcanic Lava	-	Fieldwork	Acocella et al. 2000
Newark Basin, USA	7777	14444	1.9		0.0	Basement	Open	Fieldwork	Anders and Schlische 1994
Northeast Idoho, USA	4583	18888	4.1		0.0	Basement	Fully Breached	Fieldwork	Anders and Schlische 1994
Cumbria, UK	8.33	34.72	4.2		0.0	Coal Seam	Open	Fieldwork	Barnett et al. 1987
Central Graben, North Sea	3333	5454	1.6	8181.0	2.5	Basement	-	3D Seismic	Cartwright 1991
Central Graben, North Sea	2424	1818	0.8	2727.0	1.1	Basement	-	3D Seismic	Cartwright 1991
Central Graben, North Sea	1515	1818	1.2	2727.0	1.8	Basement	-	3D Seismic	Cartwright 1991
Central Graben, North Sea	1212	2424	2.0	3636.0	3.0	Basement	-	3D Seismic	Cartwright 1991
Northern North Sea	565	1043	1.8	1564.5	2.8	Sandstone	Open	3D Seismic	Childs et al. 1995
Northern North Sea	200	650	3.3	975.0	4.9	Sandstone	-	3D Seismic	Childs et al. 1995
Northern North Sea	164	642	3.9	963.0	5.9	Sandstone	Linked	3D Seismic	Childs et al. 1995
Abruzzo, Italy	9545	17727	1.9		0.0	Basement	Open	Fieldwork	Cowie and Roberts 2001
Abruzzo, Italy	8181	27272	3.3		0.0	Basement	Open	Fieldwork	Cowie and Roberts 2001
Abruzzo, Italy	7500	13636	1.8		0.0	Basement	Open	Fieldwork	Cowie and Roberts 2001
Atalanti, Greece	1666	1666	1.0		0.0	Basement	Open	Fieldwork	Gawthorpe and Hurst 1993
Solite Quarry, NC, USA	0.0598	0.0127	0.2		0.0	Siltstone	-	Fieldwork	Gupta and Scholz 2000
Solite Quarry, NC, USA	0.0353	0.0216	0.6		0.0	Siltstone	-	Fieldwork	Gupta and Scholz 2000
Solite Quarry, NC, USA	0.034	0.0335	1.0		0.0	Siltstone	-	Fieldwork	Gupta and Scholz 2000
Solite Quarry, NC, USA	0.0326	0.0657	2.0		0.0	Siltstone	-	Fieldwork	Gupta and Scholz 2000
Solite Quarry, NC, USA	0.0289	0.0428	1.5		0.0	Siltstone	-	Fieldwork	Gupta and Scholz 2000
Solite Quarry, NC, USA	0.0217	0.0344	1.6		0.0	Siltstone	-	Fieldwork	Gupta and Scholz 2000
Solite Quarry, NC, USA	0.0202	0.0446	2.2		0.0	Siltstone	-	Fieldwork	Gupta and Scholz 2000
Solite Quarry, NC, USA	0.0188	0.0461	2.5		0.0	Siltstone	-	Fieldwork	Gupta and Scholz 2000
Solite Quarry, NC, USA	0.0179	0.0344	1.9		0.0	Siltstone	-	Fieldwork	Gupta and Scholz 2000
Solite Quarry, NC, USA	0.0173	0.0131	0.8		0.0	Siltstone	-	Fieldwork	Gupta and Scholz 2000
Solite Quarry, NC, USA	0.0162	0.0396	2.4		0.0	Siltstone	-	Fieldwork	Gupta and Scholz 2000
Solite Quarry, NC, USA	0.0152	0.0139	0.9		0.0	Siltstone	-	Fieldwork	Gupta and Scholz 2000
Solite Quarry, NC, USA	0.0137	0.0147	1.1		0.0	Siltstone	-	Fieldwork	Gupta and Scholz 2000
Solite Quarry, NC, USA	0.0136	0.0163	1.2		0.0	Siltstone	-	Fieldwork	Gupta and Scholz 2000
Solite Quarry, NC, USA	0.0134	0.0438	3.3		0.0	Siltstone	-	Fieldwork	Gupta and Scholz 2000
Solite Quarry, NC, USA	0.013	0.034	2.6		0.0	Siltstone	-	Fieldwork	Gupta and Scholz 2000
Solite Quarry, NC, USA	0.0118	0.0181	1.5		0.0	Siltstone	-	Fieldwork	Gupta and Scholz 2000
Solite Quarry, NC, USA	0.0106	0.0108	1.0		0.0	Siltstone	-	Fieldwork	Gupta and Scholz 2000

Digital Appendix

Location	Separation (m)	Overlap (m)	AR	Corrected Overlap (m)	Corrected AR	Rock Type(s)	Fault Linkage	Data Type	Data Sources
Solite Quarry, NC, USA	0.0105	0.0321	3.1	0.0		Siltstone	-	Fieldwork	Gupta and Scholz 2000
Solite Quarry, NC, USA	0.0098	0.0244	2.5	0.0		Siltstone	-	Fieldwork	Gupta and Scholz 2000
Solite Quarry, NC, USA	0.0095	0.045	4.7	0.0		Siltstone	-	Fieldwork	Gupta and Scholz 2000
Solite Quarry, NC, USA	0.009	0.0105	1.2	0.0		Siltstone	-	Fieldwork	Gupta and Scholz 2000
Solite Quarry, NC, USA	0.0083	0.0194	2.3	0.0		Siltstone	-	Fieldwork	Gupta and Scholz 2000
Solite Quarry, NC, USA	0.0078	0.0094	1.2	0.0		Siltstone	-	Fieldwork	Gupta and Scholz 2000
Solite Quarry, NC, USA	0.0072	0.0245	3.4	0.0		Siltstone	-	Fieldwork	Gupta and Scholz 2000
Solite Quarry, NC, USA	0.0071	0.0213	3.0	0.0		Siltstone	-	Fieldwork	Gupta and Scholz 2000
Solite Quarry, NC, USA	0.0071	0.0183	2.6	0.0		Siltstone	-	Fieldwork	Gupta and Scholz 2000
Solite Quarry, NC, USA	0.0071	0.02	2.8	0.0		Siltstone	-	Fieldwork	Gupta and Scholz 2000
Solite Quarry, NC, USA	0.0069	0.0162	2.3	0.0		Siltstone	-	Fieldwork	Gupta and Scholz 2000
Solite Quarry, NC, USA	0.0062	0.0055	0.9	0.0		Siltstone	-	Fieldwork	Gupta and Scholz 2000
Solite Quarry, NC, USA	0.0062	0.0276	4.5	0.0		Siltstone	-	Fieldwork	Gupta and Scholz 2000
Solite Quarry, NC, USA	0.0062	0.0235	3.8	0.0		Siltstone	-	Fieldwork	Gupta and Scholz 2000
Solite Quarry, NC, USA	0.0054	0.0334	6.2	0.0		Siltstone	-	Fieldwork	Gupta and Scholz 2000
Solite Quarry, NC, USA	0.0054	0.0219	4.1	0.0		Siltstone	-	Fieldwork	Gupta and Scholz 2000
Solite Quarry, NC, USA	0.0053	0.0084	1.6	0.0		Siltstone	-	Fieldwork	Gupta and Scholz 2000
Solite Quarry, NC, USA	0.005	0.019	3.8	0.0		Siltstone	-	Fieldwork	Gupta and Scholz 2000
Solite Quarry, NC, USA	0.0049	0.0214	4.4	0.0		Siltstone	-	Fieldwork	Gupta and Scholz 2000
Solite Quarry, NC, USA	0.0044	0.0083	1.9	0.0		Siltstone	-	Fieldwork	Gupta and Scholz 2000
Solite Quarry, NC, USA	0.0044	0.0059	1.3	0.0		Siltstone	-	Fieldwork	Gupta and Scholz 2000
Solite Quarry, NC, USA	0.0039	0.0045	1.2	0.0		Siltstone	-	Fieldwork	Gupta and Scholz 2000
Solite Quarry, NC, USA	0.0036	0.0171	4.8	0.0		Siltstone	-	Fieldwork	Gupta and Scholz 2000
Solite Quarry, NC, USA	0.0035	0.013	3.7	0.0		Siltstone	-	Fieldwork	Gupta and Scholz 2000
Solite Quarry, NC, USA	0.0034	0.0072	2.1	0.0		Siltstone	-	Fieldwork	Gupta and Scholz 2000
Solite Quarry, NC, USA	0.0033	0.0159	4.8	0.0		Siltstone	-	Fieldwork	Gupta and Scholz 2000
Solite Quarry, NC, USA	0.0025	0.0047	1.9	0.0		Siltstone	-	Fieldwork	Gupta and Scholz 2000
Solite Quarry, NC, USA	0.0024	0.0143	6.0	0.0		Siltstone	-	Fieldwork	Gupta and Scholz 2000
Solite Quarry, NC, USA	0.0024	0.0125	5.2	0.0		Siltstone	-	Fieldwork	Gupta and Scholz 2000
Solite Quarry, NC, USA	0.0023	0.0135	5.9	0.0		Siltstone	-	Fieldwork	Gupta and Scholz 2000
Solite Quarry, NC, USA	0.002	0.0075	3.8	0.0		Siltstone	-	Fieldwork	Gupta and Scholz 2000
Solite Quarry, NC, USA	0.002	0.0072	3.6	0.0		Siltstone	-	Fieldwork	Gupta and Scholz 2000
Solite Quarry, NC, USA	0.0019	0.0076	4.0	0.0		Siltstone	-	Fieldwork	Gupta and Scholz 2000
Solite Quarry, NC, USA	0.0018	0.0079	4.4	0.0		Siltstone	-	Fieldwork	Gupta and Scholz 2000
Solite Quarry, NC, USA	0.0017	0.0063	3.7	0.0		Siltstone	-	Fieldwork	Gupta and Scholz 2000
Solite Quarry, NC, USA	0.0016	0.0064	4.0	0.0		Siltstone	-	Fieldwork	Gupta and Scholz 2000
Solite Quarry, NC, USA	0.0015	0.007	4.7	0.0		Siltstone	-	Fieldwork	Gupta and Scholz 2000
Solite Quarry, NC, USA	0.0015	0.009	6.0	0.0		Siltstone	-	Fieldwork	Gupta and Scholz 2000
Solite Quarry, NC, USA	0.0014	0.0046	3.3	0.0		Siltstone	-	Fieldwork	Gupta and Scholz 2000
Solite Quarry, NC, USA	0.0013	0.0048	3.7	0.0		Siltstone	-	Fieldwork	Gupta and Scholz 2000
Solite Quarry, NC, USA	0.0013	0.0075	5.8	0.0		Siltstone	-	Fieldwork	Gupta and Scholz 2000
Solite Quarry, NC, USA	0.0009	0.0028	3.1	0.0		Siltstone	-	Fieldwork	Gupta and Scholz 2000
Solite Quarry, NC, USA	0.0008	0.0025	3.1	0.0		Siltstone	-	Fieldwork	Gupta and Scholz 2000
Solite Quarry, NC, USA	0.0008	0.0058	7.3	0.0		Siltstone	-	Fieldwork	Gupta and Scholz 2000
Solite Quarry, NC, USA	0.0007	0.0023	3.3	0.0		Siltstone	-	Fieldwork	Gupta and Scholz 2000
Solite Quarry, NC, USA	0.0006	0.0015	2.5	0.0		Siltstone	-	Fieldwork	Gupta and Scholz 2000
UK, Coal mines	230	400	1.7	0.0		Coal Seem	-	Fieldwork	Huggins et al. 1995
UK, Coal mines	72	202	2.8	0.0		Coal Seem	-	Fieldwork	Huggins et al. 1995
UK, Coal mines	72	330	4.6	0.0		Coal Seem	-	Fieldwork	Huggins et al. 1995
UK, Coal mines	61	72	1.2	0.0		Coal Seem	-	Fieldwork	Huggins et al. 1995
UK, Coal mines	53	210	4.0	0.0		Coal Seem	-	Fieldwork	Huggins et al. 1995
UK, Coal mines	49	56	1.1	0.0		Coal Seem	-	Fieldwork	Huggins et al. 1995
UK, Coal mines	49	160	3.3	0.0		Coal Seem	-	Fieldwork	Huggins et al. 1995
UK, Coal mines	49	230	4.7	0.0		Coal Seem	-	Fieldwork	Huggins et al. 1995
UK, Coal mines	49	260	5.3	0.0		Coal Seem	-	Fieldwork	Huggins et al. 1995
UK, Coal mines	49	305	6.2	0.0		Coal Seem	-	Fieldwork	Huggins et al. 1995
UK, Coal mines	43	103	2.4	0.0		Coal Seem	-	Fieldwork	Huggins et al. 1995
UK, Coal mines	43	128	3.0	0.0		Coal Seem	-	Fieldwork	Huggins et al. 1995
UK, Coal mines	42	26	0.6	0.0		Coal Seem	-	Fieldwork	Huggins et al. 1995
UK, Coal mines	41	102	2.5	0.0		Coal Seem	-	Fieldwork	Huggins et al. 1995
UK, Coal mines	33	180	5.5	0.0		Coal Seem	-	Fieldwork	Huggins et al. 1995
UK, Coal mines	33	380	11.5	0.0		Coal Seem	-	Fieldwork	Huggins et al. 1995
UK, Coal mines	29	47	1.6	0.0		Coal Seem	-	Fieldwork	Huggins et al. 1995
UK, Coal mines	29	190	6.6	0.0		Coal Seem	-	Fieldwork	Huggins et al. 1995
UK, Coal mines	25	60	2.4	0.0		Coal Seem	-	Fieldwork	Huggins et al. 1995
UK, Coal mines	25	102	4.1	0.0		Coal Seem	-	Fieldwork	Huggins et al. 1995
UK, Coal mines	24	55	2.3	0.0		Coal Seem	-	Fieldwork	Huggins et al. 1995
UK, Coal mines	23	20	0.9	0.0		Coal Seem	-	Fieldwork	Huggins et al. 1995
UK, Coal mines	23	33	1.4	0.0		Coal Seem	-	Fieldwork	Huggins et al. 1995
UK, Coal mines	23	34	1.5	0.0		Coal Seem	-	Fieldwork	Huggins et al. 1995
UK, Coal mines	23	72	3.1	0.0		Coal Seem	-	Fieldwork	Huggins et al. 1995
UK, Coal mines	23	100	4.3	0.0		Coal Seem	-	Fieldwork	Huggins et al. 1995
UK, Coal mines	23	150	6.5	0.0		Coal Seem	-	Fieldwork	Huggins et al. 1995
UK, Coal mines	21	100	4.8	0.0		Coal Seem	-	Fieldwork	Huggins et al. 1995
UK, Coal mines	20	12	0.6	0.0		Coal Seem	-	Fieldwork	Huggins et al. 1995
UK, Coal mines	20	49	2.5	0.0		Coal Seem	-	Fieldwork	Huggins et al. 1995
UK, Coal mines	20	67	3.4	0.0		Coal Seem	-	Fieldwork	Huggins et al. 1995
UK, Coal mines	20	72	3.6	0.0		Coal Seem	-	Fieldwork	Huggins et al. 1995
UK, Coal mines	20	84	4.2	0.0		Coal Seem	-	Fieldwork	Huggins et al. 1995
UK, Coal mines	20	122	6.1	0.0		Coal Seem	-	Fieldwork	Huggins et al. 1995
UK, Coal mines	20	135	6.8	0.0		Coal Seem	-	Fieldwork	Huggins et al. 1995
UK, Coal mines	17	60	3.5	0.0		Coal Seem	-	Fieldwork	Huggins et al. 1995
UK, Coal mines	17	135	7.9	0.0		Coal Seem	-	Fieldwork	Huggins et al. 1995
UK, Coal mines	16	16	1.0	0.0		Coal Seem	-	Fieldwork	Huggins et al. 1995
UK, Coal mines	16	20	1.3	0.0		Coal Seem	-	Fieldwork	Huggins et al. 1995
UK, Coal mines	16	29	1.8	0.0		Coal Seem		Fieldwork	Huggins et al. 1995
UK, Coal mines	16	72	4.5	0.0		Coal Seem	-	Fieldwork	Huggins et al. 1995
UK, Coal mines	16	120	7.5	0.0		Coal Seem	-	Fieldwork	Huggins et al. 1995
UK, Coal mines	15	7	0.5	0.0		Coal Seem	-	Fieldwork	Huggins et al. 1995
UK, Coal mines	15	12	0.8	0.0		Coal Seem	-	Fieldwork	Huggins et al. 1995

Digital Appendix

Location	Separation (m)	Overlap (m)	AR	Corrected Overlap (m)	Corrected AR	Rock Type(s)	Fault Linkage	Data Type	Data Sources
UK, Coal mines	15	120	8.0		0.0	Coal Seem	-	Fieldwork	Huggins et al. 1995
UK, Coal mines	14	11	0.8		0.0	Coal Seem	-	Fieldwork	Huggins et al. 1995
UK, Coal mines	14	23	1.6		0.0	Coal Seem	-	Fieldwork	Huggins et al. 1995
UK, Coal mines	14	72	5.1		0.0	Coal Seem	-	Fieldwork	Huggins et al. 1995
UK, Coal mines	13.5	240	17.8		0.0	Coal Seem	-	Fieldwork	Huggins et al. 1995
UK, Coal mines	13	20	1.5		0.0	Coal Seem	-	Fieldwork	Huggins et al. 1995
UK, Coal mines	13	72	5.5		0.0	Coal Seem	-	Fieldwork	Huggins et al. 1995
UK, Coal mines	12	9	0.8		0.0	Coal Seem	-	Fieldwork	Huggins et al. 1995
UK, Coal mines	12	11	0.9		0.0	Coal Seem	-	Fieldwork	Huggins et al. 1995
UK, Coal mines	12	14	1.2		0.0	Coal Seem	-	Fieldwork	Huggins et al. 1995
UK, Coal mines	12	20	1.7		0.0	Coal Seem	-	Fieldwork	Huggins et al. 1995
UK, Coal mines	12	120	10.0		0.0	Coal Seem	-	Fieldwork	Huggins et al. 1995
UK, Coal mines	11	12	1.1		0.0	Coal Seem	-	Fieldwork	Huggins et al. 1995
UK, Coal mines	11	20	1.8		0.0	Coal Seem	-	Fieldwork	Huggins et al. 1995
UK, Coal mines	11	23	2.1		0.0	Coal Seem	-	Fieldwork	Huggins et al. 1995
UK, Coal mines	11	50	4.5		0.0	Coal Seem	-	Fieldwork	Huggins et al. 1995
UK, Coal mines	11	58	5.3		0.0	Coal Seem	-	Fieldwork	Huggins et al. 1995
UK, Coal mines	11	72	6.5		0.0	Coal Seem	-	Fieldwork	Huggins et al. 1995
UK, Coal mines	9.9	4.9	0.5		0.0	Coal Seem	-	Fieldwork	Huggins et al. 1995
UK, Coal mines	9.9	110	11.1		0.0	Coal Seem	-	Fieldwork	Huggins et al. 1995
UK, Coal mines	9.9	140	14.1		0.0	Coal Seem	-	Fieldwork	Huggins et al. 1995
UK, Coal mines	9.6	14	1.5		0.0	Coal Seem	-	Fieldwork	Huggins et al. 1995
UK, Coal mines	9.6	17	1.8		0.0	Coal Seem	-	Fieldwork	Huggins et al. 1995
UK, Coal mines	9.6	23	2.4		0.0	Coal Seem	-	Fieldwork	Huggins et al. 1995
UK, Coal mines	9.6	28	2.9		0.0	Coal Seem	-	Fieldwork	Huggins et al. 1995
UK, Coal mines	9.6	31	3.2		0.0	Coal Seem	-	Fieldwork	Huggins et al. 1995
UK, Coal mines	9.5	28	2.9		0.0	Coal Seem	-	Fieldwork	Huggins et al. 1995
UK, Coal mines	8.9	10	1.1		0.0	Coal Seem	-	Fieldwork	Huggins et al. 1995
UK, Coal mines	8.8	47	5.3		0.0	Coal Seem	-	Fieldwork	Huggins et al. 1995
UK, Coal mines	7.3	4.9	0.7		0.0	Coal Seem	-	Fieldwork	Huggins et al. 1995
UK, Coal mines	7.3	12	1.6		0.0	Coal Seem	-	Fieldwork	Huggins et al. 1995
UK, Coal mines	7.2	20	2.8		0.0	Coal Seem	-	Fieldwork	Huggins et al. 1995
UK, Coal mines	7.2	23	3.2		0.0	Coal Seem	-	Fieldwork	Huggins et al. 1995
UK, Coal mines	7.2	29	4.0		0.0	Coal Seem	-	Fieldwork	Huggins et al. 1995
UK, Coal mines	7.2	34	4.7		0.0	Coal Seem	-	Fieldwork	Huggins et al. 1995
UK, Coal mines	7.2	47	6.5		0.0	Coal Seem	-	Fieldwork	Huggins et al. 1995
UK, Coal mines	6	4	0.7		0.0	Coal Seem	-	Fieldwork	Huggins et al. 1995
UK, Coal mines	5.9	12	2.0		0.0	Coal Seem	-	Fieldwork	Huggins et al. 1995
UK, Coal mines	5.9	20	3.4		0.0	Coal Seem	-	Fieldwork	Huggins et al. 1995
UK, Coal mines	5.9	23	3.9		0.0	Coal Seem	-	Fieldwork	Huggins et al. 1995
UK, Coal mines	5	4.9	1.0		0.0	Coal Seem	-	Fieldwork	Huggins et al. 1995
UK, Coal mines	4.9	7.2	1.5		0.0	Coal Seem	-	Fieldwork	Huggins et al. 1995
UK, Coal mines	4.9	10	2.0		0.0	Coal Seem	-	Fieldwork	Huggins et al. 1995
UK, Coal mines	4.8	14	2.9		0.0	Coal Seem	-	Fieldwork	Huggins et al. 1995
UK, Coal mines	4.8	23	4.8		0.0	Coal Seem	-	Fieldwork	Huggins et al. 1995
UK, Coal mines	4.8	31	6.5		0.0	Coal Seem	-	Fieldwork	Huggins et al. 1995
UK, Coal mines	4.8	41	8.5		0.0	Coal Seem	-	Fieldwork	Huggins et al. 1995
UK, Coal mines	4	10	2.5		0.0	Coal Seem	-	Fieldwork	Huggins et al. 1995
UK, Coal mines	4	38	9.5		0.0	Coal Seem	-	Fieldwork	Huggins et al. 1995
UK, Coal mines	2.3	3.6	1.6		0.0	Coal Seem	-	Fieldwork	Huggins et al. 1995
Karstryggen, Greenland	4411	5294	1.2		0.0	Basement	Open	Fieldwork	Larsen 1988
Northern North Sea	2222	3333	1.5	4999.5	2.3	Sst & Shale	Open	3D Seismic	McLeod et al. 2000
Northern North Sea	1470	2941	2.0	4411.5	3.0	Sst & Shale	Open	3D Seismic	McLeod et al. 2000
Northern North Sea	1111	1666	1.5	2499.0	2.2	Sst & Shale	Open	3D Seismic	McLeod et al. 2000
Kenya	3684	4210	1.1	6315.0	1.7	Sst & Shale	Open	3D Seismic	Morley 2002
North Sea Rift	29268	58536	2.0		0.0	Basement	-	Fieldwork	Morley et al. 1990
North Sea Rift	12195	24390	2.0		0.0	Basement	-	Fieldwork	Morley et al. 1990
North Sea Rift	4000	9600	2.4		0.0	Basement	-	Fieldwork	Morley et al. 1990
Hawaii	689	1034	1.5		0.0	Volcanic Lava	Open	Fieldwork	Peacock and Parfitt 2002
Hawaii	603	1379	2.3		0.0	Volcanic Lava	Fully Breached	Fieldwork	Peacock and Parfitt 2002
Kilve, Somerset, UK	0.26	0.9	3.5		0.0	Carbonate	Linked	Fieldwork	Peacock et al. 1994
Kilve, Somerset, UK	0.15	0.9	6.0		0.0	Carbonate	Fully Breached	Fieldwork	Peacock et al. 1994
Kilve, Somerset, UK	0.14	0.64	4.6		0.0	Carbonate	Linked	Fieldwork	Peacock et al. 1994
Kilve, Somerset, UK	0.08	0.75	9.4		0.0	Carbonate	Open	Fieldwork	Peacock et al. 1994
Kilve, Somerset, UK	0.03	0.27	9.0		0.0	Carbonate	Linked	Fieldwork	Peacock et al. 1994
Greenland	100000	250000	2.5		0.0	Basement	-	Fieldwork	Peacock et al. 2000
Gulf of Corinth, Greece	1666	5416	3.3		0.0	Carbonate	Open	Fieldwork	Roberts and Jackson 1991
Gulf of Corinth, Greece	1250	2083	1.7		0.0	Carbonate	Open	Fieldwork	Roberts and Jackson 1991
Gulf of Corinth, Greece	833	2500	3.0		0.0	Carbonate	Open	Fieldwork	Roberts and Jackson 1991
Gulf of Corinth, Greece	833	1666	2.0		0.0	Carbonate	Open	Fieldwork	Roberts and Jackson 1991
Fumanya, Spain	0.238	0.63	2.6		0.0	Carbonate	Open	Fieldwork	Soliva and Benedicto 2004
Fumanya, Spain	0.225	0.8	3.6		0.0	Carbonate	Linked	Fieldwork	Soliva and Benedicto 2004
Niguelas, Spain	0.197	0.91	4.6		0.0	Carbonate	Linked	Fieldwork	Soliva and Benedicto 2004
Niguelas, Spain	0.177	0.75	4.2		0.0	Carbonate	Open	Fieldwork	Soliva and Benedicto 2004
Fumanya, Spain	0.142	0.75	5.3		0.0	Carbonate	Fully Breached	Fieldwork	Soliva and Benedicto 2004
Fumanya, Spain	0.139	0.8	5.8		0.0	Carbonate	Linked	Fieldwork	Soliva and Benedicto 2004
Niguelas, Spain	0.135	1.05	7.8		0.0	Carbonate	Fully Breached	Fieldwork	Soliva and Benedicto 2004
Fumanya, Spain	0.13	0.6	4.6		0.0	Carbonate	Linked	Fieldwork	Soliva and Benedicto 2004
Fumanya, Spain	0.123	0.42	3.4		0.0	Carbonate	Linked	Fieldwork	Soliva and Benedicto 2004
Fumanya, Spain	0.117	0.2	1.7		0.0	Carbonate	Open	Fieldwork	Soliva and Benedicto 2004
Niguelas, Spain	0.107	0.2	1.9		0.0	Carbonate	Open	Fieldwork	Soliva and Benedicto 2004
Fumanya, Spain	0.083	0.45	5.4		0.0	Carbonate	Linked	Fieldwork	Soliva and Benedicto 2004
Niguelas, Spain	0.076	0.23	3.0		0.0	Carbonate	Fully Breached	Fieldwork	Soliva and Benedicto 2004
Niguelas, Spain	0.07	0.5	7.1		0.0	Carbonate	Fully Breached	Fieldwork	Soliva and Benedicto 2004
Fumanya, Spain	0.068	0.32	4.7		0.0	Carbonate	Fully Breached	Fieldwork	Soliva and Benedicto 2004
Fumanya, Spain	0.065	0.1	1.5		0.0	Carbonate	Fully Breached	Fieldwork	Soliva and Benedicto 2004
Niguelas, Spain	0.0645	0.195	3.0		0.0	Carbonate	Open	Fieldwork	Soliva and Benedicto 2004
Niguelas, Spain	0.058	0.825	14.2		0.0	Carbonate	Fully Breached	Fieldwork	Soliva and Benedicto 2004
Niguelas, Spain	0.05	0.29	5.8		0.0	Carbonate	Fully Breached	Fieldwork	Soliva and Benedicto 2004
Fumanya, Spain	0.048	0.83	17.3		0.0	Carbonate	Linked	Fieldwork	Soliva and Benedicto 2004

Location	Separation (m)	Overlap (m)	AR	Corrected Overlap (m)	Corrected AR	Rock Type(s)	Fault Linkage	Data Type	Data Sources
Niguelas, Spain	0.043	0.18	4.2		0.0	Carbonate	Open	Fieldwork	Soliva and Benedicto 2004
Niguelas, Spain	0.036	0.11	3.1		0.0	Carbonate	Linked	Fieldwork	Soliva and Benedicto 2004
Niguelas, Spain	0.035	0.1	2.9		0.0	Carbonate	Fully Breached	Fieldwork	Soliva and Benedicto 2004
Niguelas, Spain	0.033	0.105	3.2		0.0	Carbonate	Fully Breached	Fieldwork	Soliva and Benedicto 2004
Fumanya, Spain	0.03	0.17	5.7		0.0	Carbonate	Fully Breached	Fieldwork	Soliva and Benedicto 2004
Fumanya, Spain	0.03	0.25	8.3		0.0	Carbonate	Fully Breached	Fieldwork	Soliva and Benedicto 2004
Niguelas, Spain	0.028	0.21	7.5		0.0	Carbonate	Fully Breached	Fieldwork	Soliva and Benedicto 2004
Niguelas, Spain	0.028	0.24	8.6		0.0	Carbonate	Fully Breached	Fieldwork	Soliva and Benedicto 2004
Fumanya, Spain	0.023	0.1	4.3		0.0	Carbonate	Fully Breached	Fieldwork	Soliva and Benedicto 2004
Fumanya, Spain	0.022	0.09	4.1		0.0	Carbonate	Open	Fieldwork	Soliva and Benedicto 2004
Fumanya, Spain	0.022	0.15	6.8		0.0	Carbonate	Fully Breached	Fieldwork	Soliva and Benedicto 2004
Niguelas, Spain	0.022	0.16	7.3		0.0	Carbonate	Fully Breached	Fieldwork	Soliva and Benedicto 2004
Niguelas, Spain	0.015	0.1	6.7		0.0	Carbonate	Fully Breached	Fieldwork	Soliva and Benedicto 2004
Niguelas, Spain	0.012	0.06	5.0		0.0	Carbonate	Open	Fieldwork	Soliva and Benedicto 2004
Niguelas, Spain	0.01	0.04	4.0		0.0	Carbonate	Open	Fieldwork	Soliva and Benedicto 2004
Aegean Region	100	220	2.2		0.0	Carbonate	Open	Fieldwork	Stewart and Hancock 1991
Aegean Region	80	220	2.8		0.0	Carbonate	Fully Breached	Fieldwork	Stewart and Hancock 1991
Canyonlands, UT, USA	140	360	2.6		0.0	Sandstone	Open	Fieldwork	Trudgill and Cartwright 1994
Canyonlands, UT, USA	120	360	3.0		0.0	Sandstone	Open	Fieldwork	Trudgill and Cartwright 1994
Canyonlands, UT, USA	66.67	100	1.5		0.0	Sandstone	-	Fieldwork	Trudgill and Cartwright 1994
Northern North Sea	250	1200	4.8	1800.0	7.2	Sst & Shale	Linked	3D Seismic	Walsh et al. 1999
Northern North Sea	133	1444	10.9	1999.5	15.0	Sst & Shale	Open	3D Seismic	Walsh et al. 1999
Northern North Sea	44.44	122	2.7	183.0	4.1	Sst & Shale	Linked	3D Seismic	Walsh et al. 1999